

LA-4780 (ENDF-174)

**c. 3**

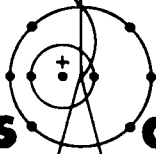
**CIC-14 REPORT COLLECTION  
REPRODUCTION  
COPY**

A Preliminary Evaluation of the Neutron  
and Photon-Production Cross Sections  
of Oxygen

LOS ALAMOS NATIONAL LABORATORY



3 9338 00320 0259



**los alamos  
scientific laboratory**

of the University of California

LOS ALAMOS, NEW MEXICO 87544



This report was prepared as an account of work sponsored by the United States Government. Neither the United States nor the United States Atomic Energy Commission, nor any of their employees, nor any of their contractors, subcontractors, or their employees, makes any warranty, express or implied, or assumes any legal liability or responsibility for the accuracy, completeness or usefulness of any information, apparatus, product or process disclosed, or represents that its use would not infringe privately owned rights.

Printed in the United States of America. Available from  
National Technical Information Service  
U. S. Department of Commerce  
5285 Port Royal Road  
Springfield, Virginia 22151  
Price: Printed Copy \$3.00; Microfiche \$0.95

LA-4780 (ENDF-174)

UC-34

ISSUED: August 1972



# A Preliminary Evaluation of the Neutron and Photon-Production Cross Sections of Oxygen

by

D. G. Foster, Jr.  
P. G. Young



This work was supported by the Defense Nuclear Agency under Subtask PC-102



TABLE OF CONTENTS

	<u>Page</u>
ABSTRACT	1
1. INTRODUCTION	1
2. NEUTRON AND PHOTON-PRODUCTION CROSS SECTIONS	2
2.1 Total Cross Section	2
2.2 Radiative Capture Cross Section	6
2.3 Inelastic Scattering Cross Sections	6
2.3.1 The $^{16}\text{O}(n,n')$ and $^{16}\text{O}(n,n'\gamma)$ Cross Sections for $E_x(^{16}\text{O}) < 13$ MeV	6
2.3.2 The $^{16}\text{O}(n,n')$ Cross Section for $E_x(^{16}\text{O}) > 13$ MeV	13
2.4 The $^{16}\text{O}(n,p)^{16}\text{N}$ and $^{16}\text{O}(n,py)^{16}\text{N}$ Cross Sections	13
2.5 The $^{16}\text{O}(n,d)^{15}\text{N}$ Cross Section	15
2.6 The $^{16}\text{O}(n,\alpha)^{13}\text{C}$ and $^{16}\text{O}(n,\alpha\gamma)^{13}\text{C}$ Cross Sections	15
2.7 Elastic Scattering Cross Section	21
3. ANGULAR DISTRIBUTIONS	22
3.1 Elastic Neutron Angular Distributions	22
3.2 Inelastic Neutron Angular Distributions	24
3.3 Secondary-Photon Angular Distributions	25
4. DISCUSSION	25
5. ACKNOWLEDGMENTS	27
REFERENCES	27

A PRELIMINARY EVALUATION OF THE NEUTRON AND  
PHOTON-PRODUCTION CROSS SECTIONS OF OXYGEN

by

D. G. Foster, Jr., and P. G. Young

ABSTRACT

A preliminary evaluation of the neutron-induced cross sections of  $^{16}\text{O}$  has been completed for the energy region  $10^{-5}$  eV to 20 MeV. Energy and angular distributions of secondary neutrons and photons are included. The recommended data are based mainly on experiment, although model calculations were used to augment the measurements in certain areas. In addition, results from an earlier evaluation performed at the Knolls Atomic Power Laboratory are also included to a limited extent. The evaluated data are available on magnetic tape in ENDF/B(III) format.

1. INTRODUCTION

A preliminary evaluation of the neutron and photon-production cross sections of oxygen has been completed for the energy range  $10^{-5}$  eV to 20 MeV. Except in the region of the "window" at 2.35 MeV, natural oxygen is treated entirely as  $^{16}\text{O}$ , and the 0.23% of  $^{17}\text{O}$  and  $^{18}\text{O}$  is ignored. The data are in ENDF/B (III) format as MAT 1134 and have been provided to the Radiation Shielding Information Center at Oak Ridge and to the National Neutron Cross Section Center at Brookhaven.

The primary purpose of this work is to provide the Defense Nuclear Agency with an interim set of cross-section data which contains a consistent set of evaluated inelastic-neutron and photon-production cross sections and which includes consideration of several important new measurements. A complete literature survey was not performed for this study, although many new measurements are included. Parts of the 1965 evaluation by Slaggie and Reynolds (S165) at the Knolls Atomic Power Laboratory (KAPL) have been incorporated in the evaluation. The present study is incomplete in several areas and should be regarded as preliminary.

A survey of the reactions of interest is given schematically in Fig. 1 (Aj59, Aj70, Aj71). The  $(n, \gamma)$  reaction has been omitted from Fig. 1 because it is very small above the electron-volt region and can be neglected for most purposes. The Q-values and thresholds for various  $n+^{16}\text{O}$  reactions are given in Table I.

The only significant channel below the  $(n, \alpha_0)$  threshold at 2.354 MeV is elastic scattering, and in practice the Coulomb barrier inhibits the  $(n, \alpha_0)$  reaction up to almost 4 MeV. Similarly, the 3.09-MeV photon from the  $(n, \alpha_1)$  reaction to the first excited state of  $^{13}\text{C}$  does not become detectable until above 7 MeV, although its threshold occurs at 5.64 MeV. Above 7 MeV, inelastic scattering is the dominant reaction channel. Although the  $(n, n'\alpha)$  channel opens at 7.61 MeV, parity conservation inhibits the levels in  $^{16}\text{O}$  below 9 MeV excitation from decaying by alpha emission, and the  $(n, n'\alpha)$  reaction does not become significant until above 11 MeV. At energies above 12.89 MeV, proton emission from excited states in  $^{16}\text{O}$  competes with alpha emission; however, at all energies the  $(n, n'p)$  reaction remains less important than the  $(n, n'\alpha)$  reaction. In this study the  $(n, n'p)$  and  $(n, n'\alpha)$

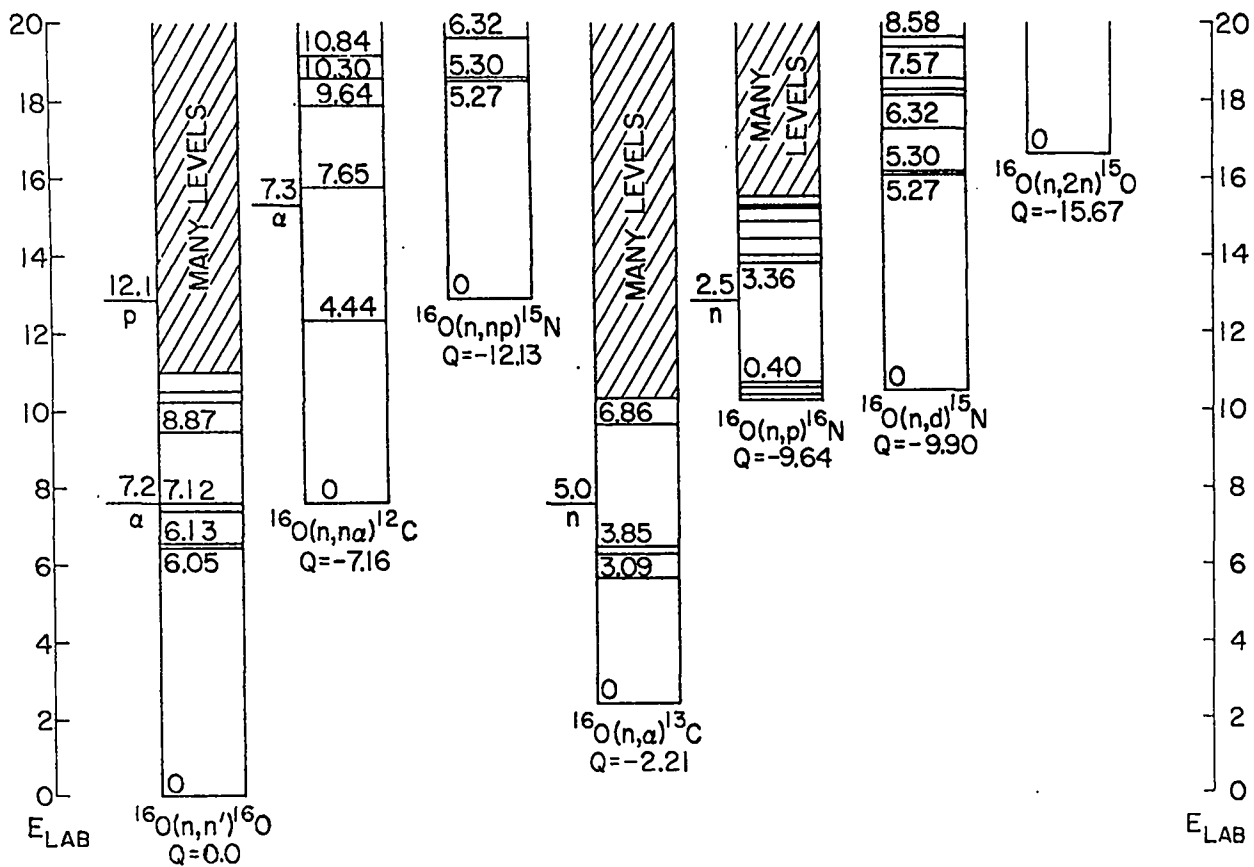


Fig. 1. Composite energy-level diagram for the residual nuclei of major interest formed in  $n + ^{16}\text{O}$  reactions. Except for the " $E_{\text{lab}}$ " scales, the energies are in the center-of-mass system, and all energies are given in MeV.

reactions are included in the discrete  $(n,n')$  ENDF/B files, with appropriate flags to indicate particle emission from the residual  $^{16}\text{O}$  excited states.

The threshold for the  $(n,p)$  reaction occurs at 10.25 MeV, followed closely by the  $(n,d)$  threshold at 10.53 MeV. The latter reaction is relatively unimportant, as its cross section is less than 16 mb at all energies. The cross section for the  $(n,2n)$  reaction is less than 3 mb below 20 MeV (Br61), and it is not included in the evaluation. Similarly, the  $(n,t)$ ,  $(n,^3\text{He})$ , and  $(n,2\alpha)$  reactions listed in Table I are expected to have very small cross sections and have been ignored.

The neutron total cross section was obtained at all energies from experimental data. Below 11 MeV, the elastic cross section was determined by subtracting the sum of all reaction cross sections, which were determined mainly from measurements, from the evaluated total cross section. Between 11 and

14 MeV, increasing emphasis was placed on the measured elastic cross section, and above 14 MeV the nonelastic cross section was determined by subtraction of the elastic from the total. The nonelastic cross section was extended to 20 MeV by optical model calculations. Above 14 MeV the  $(n,p)$ ,  $(n,d)$ , and  $(n,\alpha)$  cross sections were taken from measurements, and the  $(n,n')$  cross section to highly excited states of  $^{16}\text{O}$  was adjusted to give the correct nonelastic cross section.

## 2. NEUTRON AND PHOTON-PRODUCTION CROSS SECTIONS

### 2.1 Total Cross Section

The total cross section has been completely re-evaluated. Because our main purpose was to incorporate recent measurements, we gave less attention to the older work, especially in the million-electron-volt region. Below 700 keV, however, the evaluated total cross section is based entirely on

TABLE I  
Q-VALUE<sup>a</sup> AND THRESHOLD FOR  
SEVERAL n+<sup>16</sup>O INTERACTIONS

Reaction	Q (MeV)	Threshold (MeV)
$^{16}_0(n,n)^{16}_0$	0	0
$^{16}_0(n,n')^{16}_0^*$	-6.050	6.432
$^{16}_0(n,\gamma)^{17}_0$	+4.143	0
$^{16}_0(n,p)^{16}_N$	-9.639	10.247
$^{16}_0(n,d)^{15}_N$	-9.901	10.526
$^{16}_0(n,t)^{14}_N$	-14.479	15.392
$^{16}_0(n,^3\text{He})^{14}_C$	-14.616	15.538
$^{16}_0(n,\alpha)^{13}_C$	-2.214	2.354
$^{16}_0(n,n'\alpha)^{12}_C$	-7.161	7.613
$^{16}_0(n,n'p)^{15}_N$	-12.126	12.891
$^{16}_0(n,2n)^{15}_0$	-15.668	16.656
$^{16}_0(n,2\alpha)^9\text{Be}$	-12.865	13.676

<sup>a</sup>All Q-values used in this evaluation are taken from the 1964 mass tables of Mattach et al. (Ma65).

very old measurements. From a preliminary approximate fit to the data of Okazaki (Ok55), the first resonance was found to have  $E_r = 442$  keV,  $\sigma_0 = 13.05$  b, and  $\Gamma = 48$  keV, all in the laboratory system. By subtracting the tail of the resonance from three measurements below 250 keV (Ad49, Jo48, Me49), we obtained a weighted average of  $3.666 \pm 0.015$  b for the low-energy potential-scattering cross section. If the (n, $\gamma$ ) cross section is assumed to vary as  $1/v$  from Journey's value (Ju71) of 178  $\mu\text{b}$  at 2200 m/sec, it contributes an additional 9 mb to the total cross section at  $10^{-5}$  eV, but is negligible above the electron-volt region. The potential-scattering background was assumed to vary linearly in the neighborhood of the 442-keV resonance in such a manner that the total cross section joins smoothly at 700 keV onto the curve deduced at higher energies. The result is shown in Figs. 2 and 3, together with the data. Near 300 keV the total cross section is a few percent higher than the KAPL evaluation.

The remainder of the evaluated total cross section is based primarily on three major time-of-flight measurements which have become available

since the 1965 evaluation. The measurement of Foster and Glasgow (Fo71) had the poorest resolution and the least reliable energy scale (especially below 3.5 MeV), but was part of an extensive series of systematic measurements which allows additional comparisons to be made with other work on other elements. It agrees with the results of Schwartz (Sc71) within about 0.5%, on the average, in the overlap interval of 2.25 to 15 MeV. Since the two measurements used different samples ( $\text{B}_2\text{O}_3$ -2B and  $\text{SiO}_2$ -Si, respectively), and similarly good agreement has been observed previously in nitrogen (Yo72) and aluminum (Yo72a), the Foster and Glasgow and the Schwartz measurements were adopted as standards for the million-electron-volt region.

The measurement by Cierjacks et al. (Ci68), who used  $\text{Al}_2\text{O}_3$  with an aluminum blank, is the only one of the original 1968 group of Karlsruhe measurements that has not subsequently been assigned a recorection for dead-time errors, and it is believed to be correct within about 20 mb at all energies above 700 keV (Ci71). However, the Cierjacks data disagree with other time-of-flight measurements in much the same way as Young and Foster (Yo72a) observed for aluminum (after recorection), namely, there is a smooth variation ranging between 1% lower and 4% higher than the Foster and Glasgow (Fo71) and Schwartz (Sc71) results. Agreement is within 1% at almost all energies when a correction similar to that used for aluminum (Yo72a) is applied.

The evaluated cross section from 0.7 to 12 MeV was taken directly from Schwartz's work (Sc71). However, since the Karlsruhe results had the best resolution of the three time-of-flight measurements, we used inserts of those results, normalized by the correction discussed above, wherever necessary to preserve the resolution. Between 12 and 20 MeV we used a composite of the work of Schwartz and Cierjacks. Below 4 MeV, the extremely narrow resonances found in the work of Fowler and Johnson (Fo70, Jo67) were corrected for resolution and superimposed on the base provided by the time-of-flight work. Unfortunately, we overlooked the fact that the earlier work of Fossan et al. (Fo61), which was the primary basis for the 1965 evaluation above 4 MeV, had

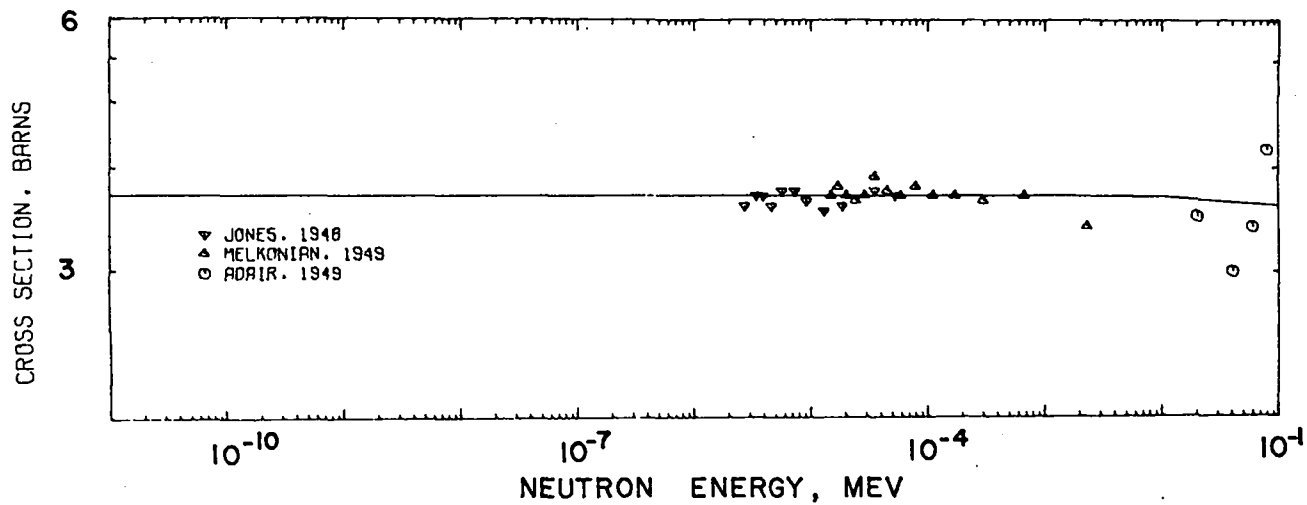


Fig. 2. Measured and evaluated total cross section for  $^{16}\text{O}$  below 0.1 MeV.

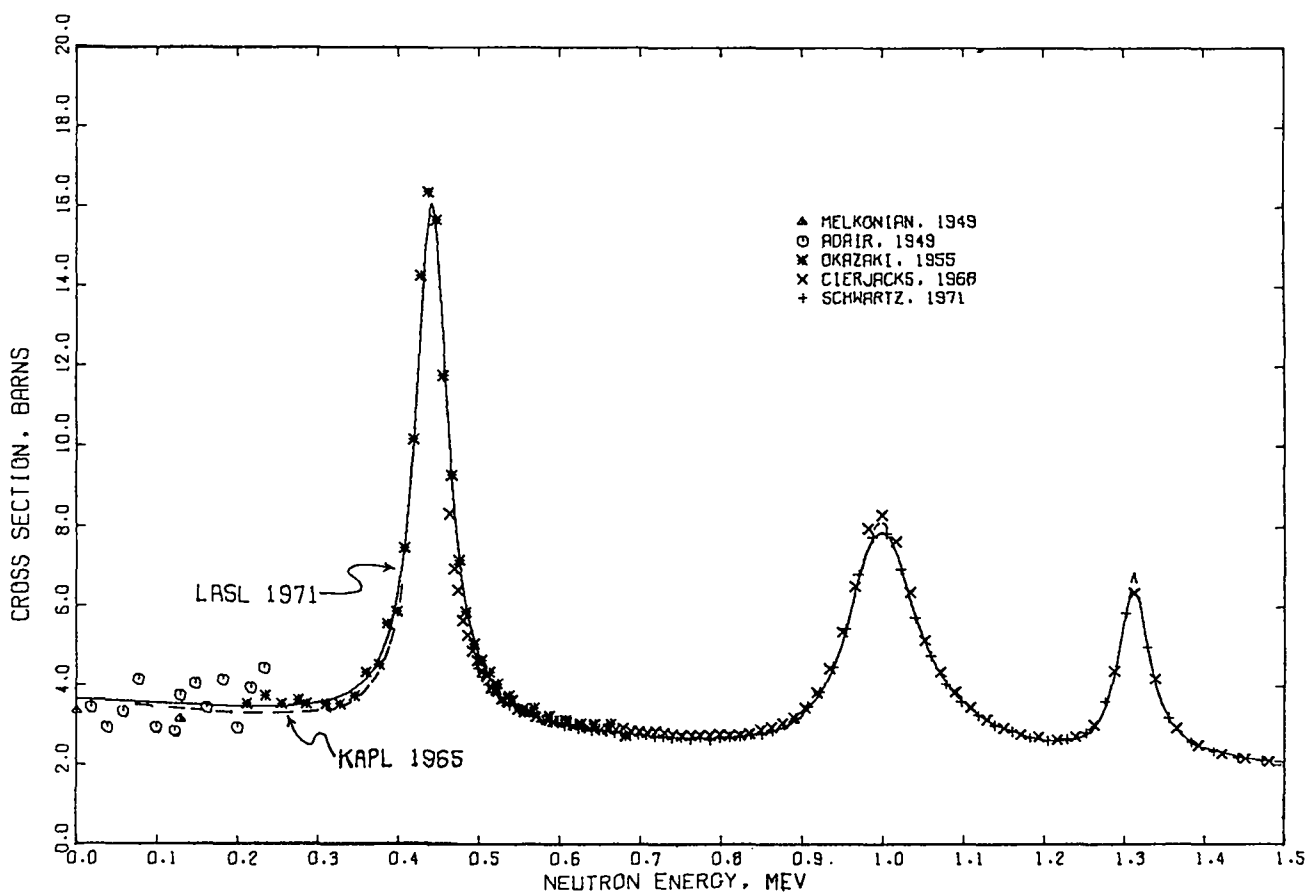


Fig. 3. Measured and evaluated total cross section for  $^{16}\text{O}$  from 0.01 to 1.5 MeV. The experimental points shown are averages of 35 points for the Cierjacks data (C168) and 25 points for the Schwartz data (Sc71).

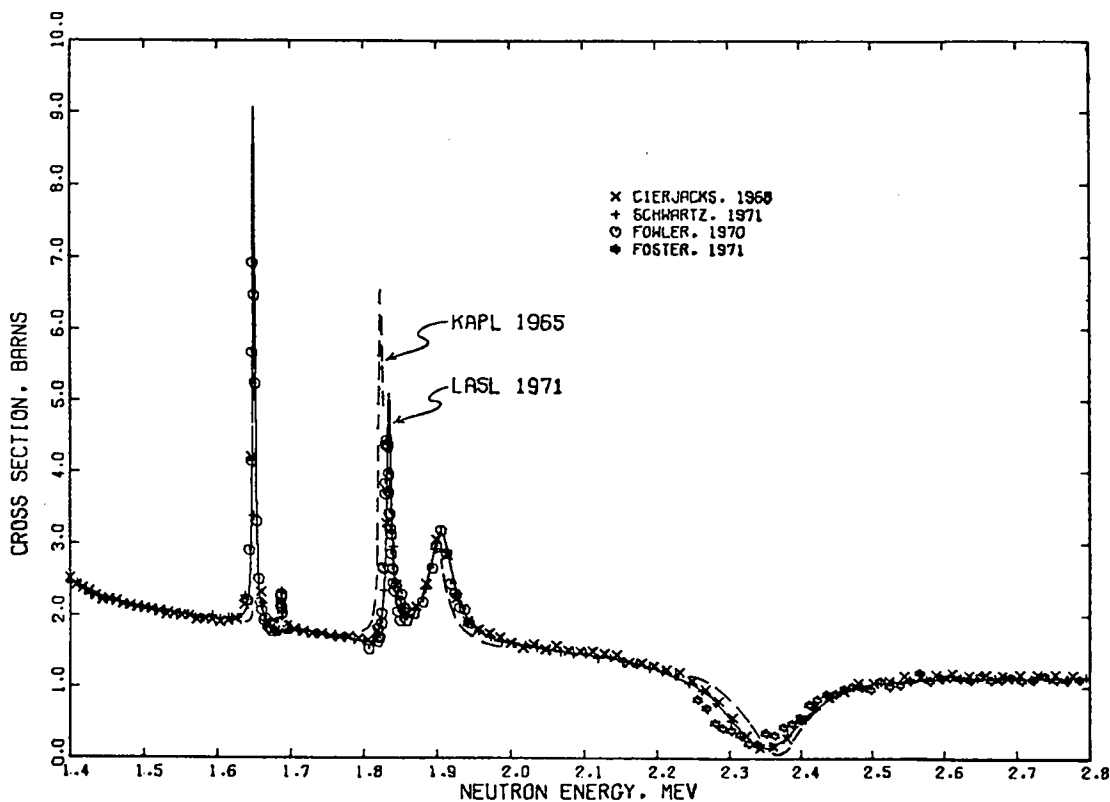


Fig. 4. Measured and evaluated total cross section for O from 1.4 to 2.8 MeV. The experimental points shown are averages of 11 points for the Cierjacks data (Ci68) and 8 points for the Schwartz data (Sc71).

better resolution\* at some energies than the work of Cierjacks, although it differs from the recent time-of-flight measurements in absolute cross section, especially at higher energies. Therefore, although the present evaluation should be more accurate in energy and absolute cross section, in isolated areas above 4 MeV its resolution is inferior to the 1965 evaluation.

Figure 4 shows the measured and evaluated cross section between 1.4 and 2.8 MeV, including the "window" in the total cross section near 2.35 MeV. An energy shift between the older and more recent work is clearly visible at the 1.83-MeV resonance. For the window itself, two additional measurements were considered. After we applied corrections for resolution ranging from 80 mb (Fo71)

to negligible (Ci68), we found that a value of  $130 \pm 10$  mb for the minimum cross section of natural oxygen agreed with the three time-of-flight measurements and Fowler's (Fo71a) point-by-point work.\* Four different samples had been used for the four measurements (Fowler et al. used BeO-Be). We rejected, for the present, a preliminary result of  $65 \pm 15$  mb made by Kalyna et al. (Ka71), who used a 5-ft-long sample of liquid oxygen. Later values reported by this group are higher and should be incorporated in the next evaluation. The present evaluation gives a window which is broader and shallower than that of the 1965 evaluation and which appears at a slightly lower energy (Fig. 4).

\* Note that in Figs. 3-7 the data of Cierjacks and Schwartz are plotted as averages of many adjacent points. This expedient introduces a further degradation of resolution in the figures but not in the evaluation.

\* Final corrections were not made until after we completed the evaluation; the total cross section at the minimum in the ENDF/B (III) data set is 139 mb.

Figures 5-7 show the evaluated total cross section in the energy range from 2.6-20 MeV, together with the data used for the present evaluation and the measurement of Fossan et al. (Fo61), which was not used. The loss of resolution can be seen at several energies. At about 8 MeV, the newer measurements and the present evaluation show a steady rise over the Fossan data and the 1965 evaluation. Near 14 MeV there is a 12% difference which has an appreciable effect on air-transport calculations for 14-MeV neutrons. In addition, some of the proportionately larger changes in the elastic cross section discussed in Sec. 2.7 are due to subtraction from this higher total cross section.

## 2.2. Radiative Capture Cross Section

For the  $^{16}\text{O}(n,\gamma)^{17}\text{O}$  cross section for thermal neutrons, we used the Journey and Motz (Ju63) value of 232  $\mu\text{b}$ . The cross section at all other neutron energies was assumed to vary as  $1/v$  from the thermal value. This assumption results in an  $(n,\gamma)$  cross section that is too small in the region of the inverse photonuclear giant resonance. However, the

actual cross section in the million-electron-volt region is undoubtedly too low to be of interest in most practical problems.

The capture gamma-ray spectrum for thermal neutrons was obtained from the measurements of Journey (Ju71) and is given schematically in Fig. 8. The total multiplicity for thermal neutrons is 2.854 photons per capture.

## 2.3. Inelastic Scattering Cross Sections

### 2.3.1. The $^{16}\text{O}(n,n')$ and $^{16}\text{O}(n,n'\gamma)$ Cross Sections for $E_x(^{16}\text{O}) < 13$ MeV. The

$(n,n')$  cross sections to the most important photon-producing levels in  $^{16}\text{O}$  were determined mainly from  $(n,n'\gamma)$  measurements. The level decay scheme for  $^{16}\text{O}$  which relates the  $(n,n')$  and  $(n,n'\gamma)$  cross sections was obtained from the compilations of Ajzenberg-Selove (Aj59, Aj70) and is given in Fig. 9. The photon transitions included in the evaluation are given in Table II.

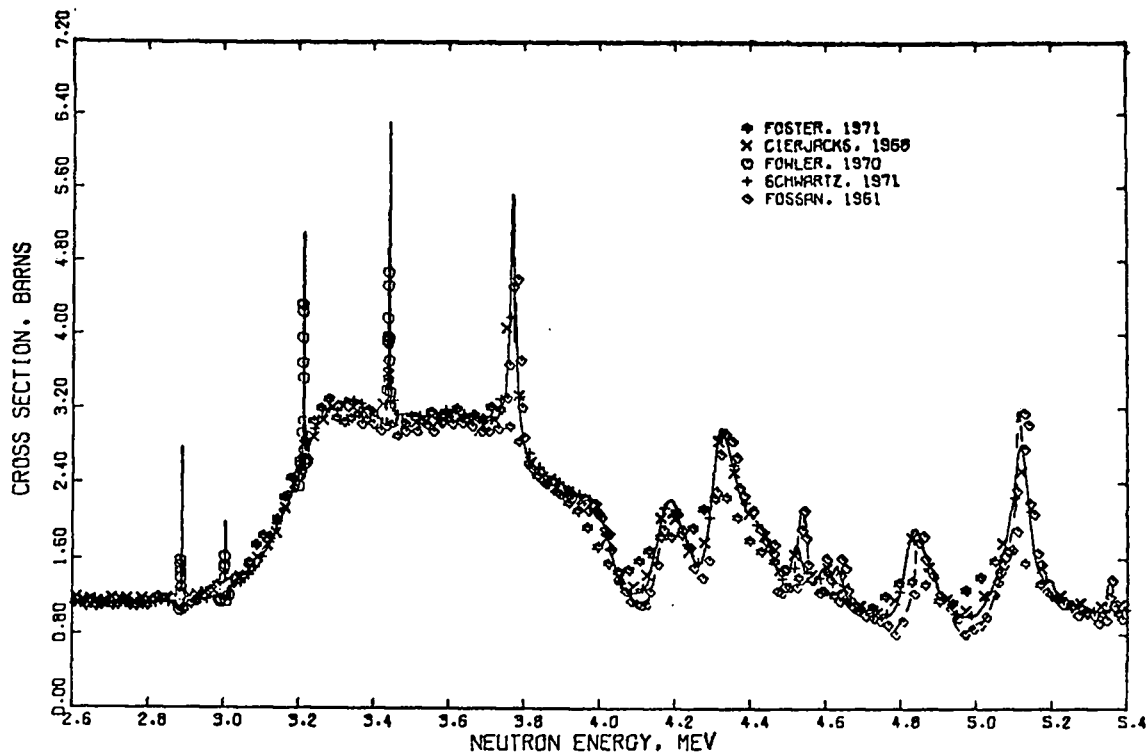


Fig. 5. Measured and evaluated total cross section for  $^{16}\text{O}$  from 2.6 to 5.4 MeV. The experimental points shown are averages of 9 points for the Cierjacks data (Ci68) and 5 points for the Schwartz data (Sc71).

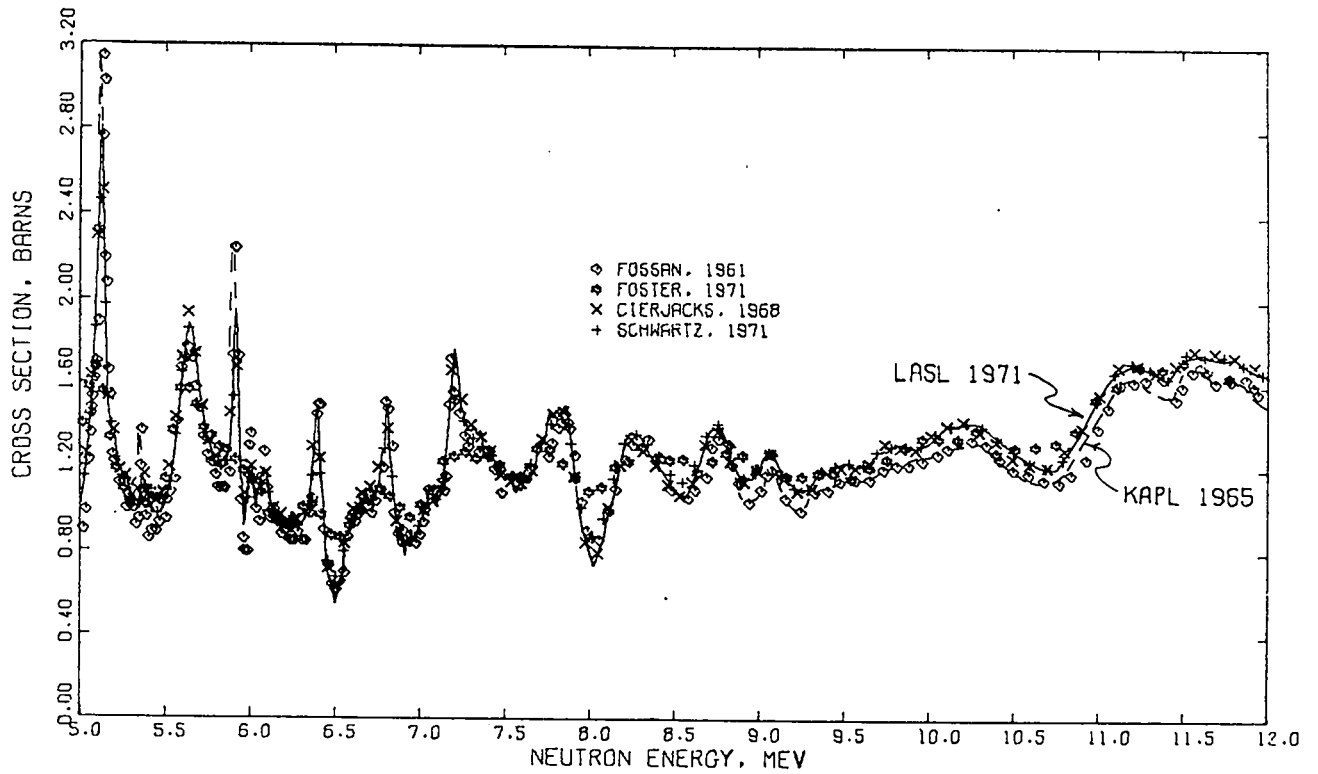


Fig. 6. Measured and evaluated total cross section for  $^{16}\text{O}$  from 5.0 to 12.0 MeV. The experimental points shown are averages of 6 points for the Cierjacks data (Ci68) and 4 points for the Schwartz data (Sc71).

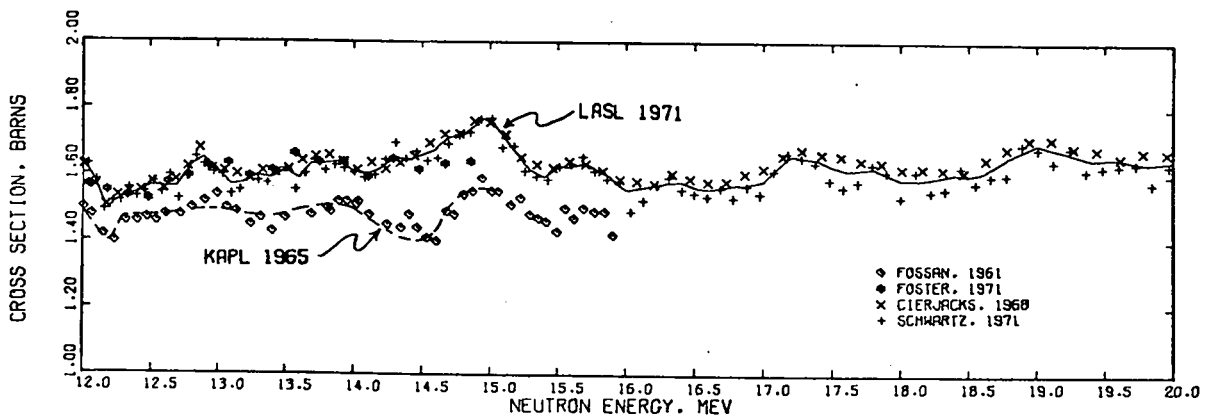


Fig. 7. Measured and evaluated total cross section for  $^{16}\text{O}$  from 12.0 to 20.0 MeV. The experimental points shown are averages of 4 points for the Cierjacks data (Ci68) and 2 points for the Schwartz data (Sc71).

TABLE II  
GAMMA RAYS FROM  
 $^{16}\text{O}(n,n'\gamma)^{16}\text{O}$  REACTIONS

$E_\gamma$ (MeV)	$E_{\text{initial}}$ (MeV)	$E_{\text{final}}$ (MeV)
8.872	8.872	0
7.119	7.119	0
6.917	6.917	0
6.131	6.131	0
4.949	11.080	6.131
4.163	11.080	6.917
3.833	10.952	7.119
2.741	8.872	6.131
2.208	11.080	8.872
1.955	8.872	6.917
1.753	8.872	7.119
0.510 <sup>a</sup>	6.050	0

<sup>a</sup>Each 6.050 $\rightarrow$ 0 transition is assumed to produce two 0.51-MeV annihilation photons.

The  $^{16}\text{O}$  nucleus has two peculiar properties that should be noted. First, the 6.050-MeV first excited state has  $J^\pi = 0^+$  and can therefore decay to the  $0^+$  ground state only by internal pair-production. Since provision has not been made in the ENDF/B system to indicate prompt electron decay following (n,n') reactions, we were not able to include in the ENDF/B files the energy deposited by the electron-positron pair. The annihilation photons from the positron, however, do appear in the photon-production files with the appropriate threshold and cross section.

The second property of  $^{16}\text{O}$  that should be noted deals with the relatively low threshold for the (n,n' $\alpha$ ) reaction. States above 7.161-MeV excitation are unstable to alpha emission (see Fig. 9); however, because both  $^{12}\text{C}$  and the alpha particle have  $0^+$  ground states, only states in  $^{16}\text{O}$  with parity equal to  $(-1)^J$  can decay to the ground state of  $^{12}\text{C}$ . The 8.872-, 10.952-, and 11.080-MeV states do not satisfy this criterion and therefore de-excite by photon emission. Thus, the (n,n' $\alpha$ ) reaction is unimportant below 10 MeV although its threshold occurs at 7.61 MeV. Above 11.605-MeV excitation, states in  $^{16}\text{O}$  can alpha-decay to the  $2^+$  first-excited level of  $^{12}\text{C}$  without the above restriction, and we have assumed that states in this region decay 100% by particle emission.

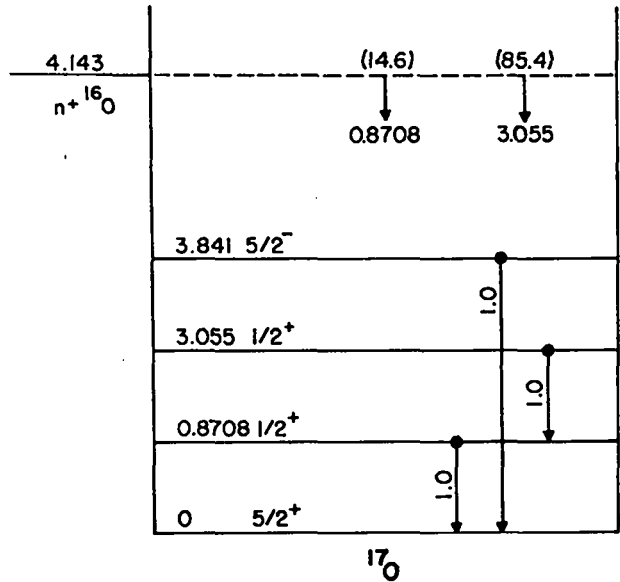


Fig. 8. Decay scheme and branching ratios for  $^{17}\text{O}$ . The transitions that occur following thermal neutron captures are given in parentheses at the top of the diagram in photons per 100 captures.

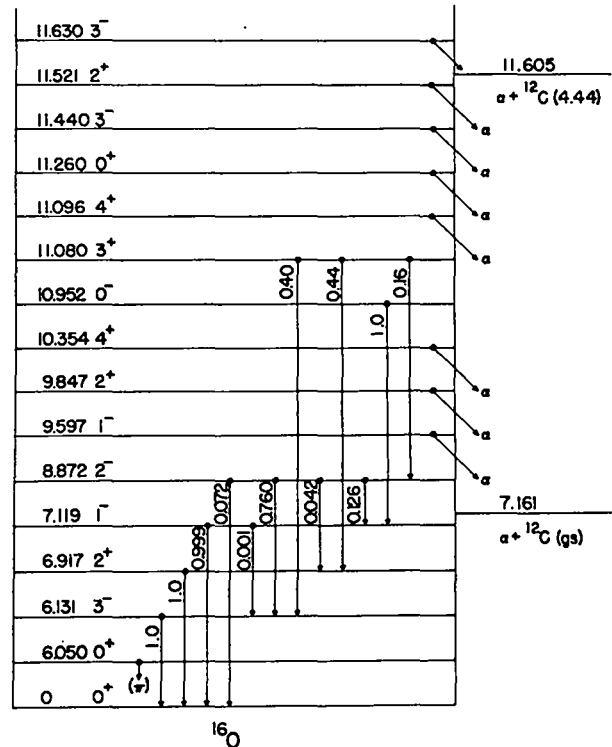


Fig. 9. Energy level decay scheme for  $^{16}\text{O}$ .

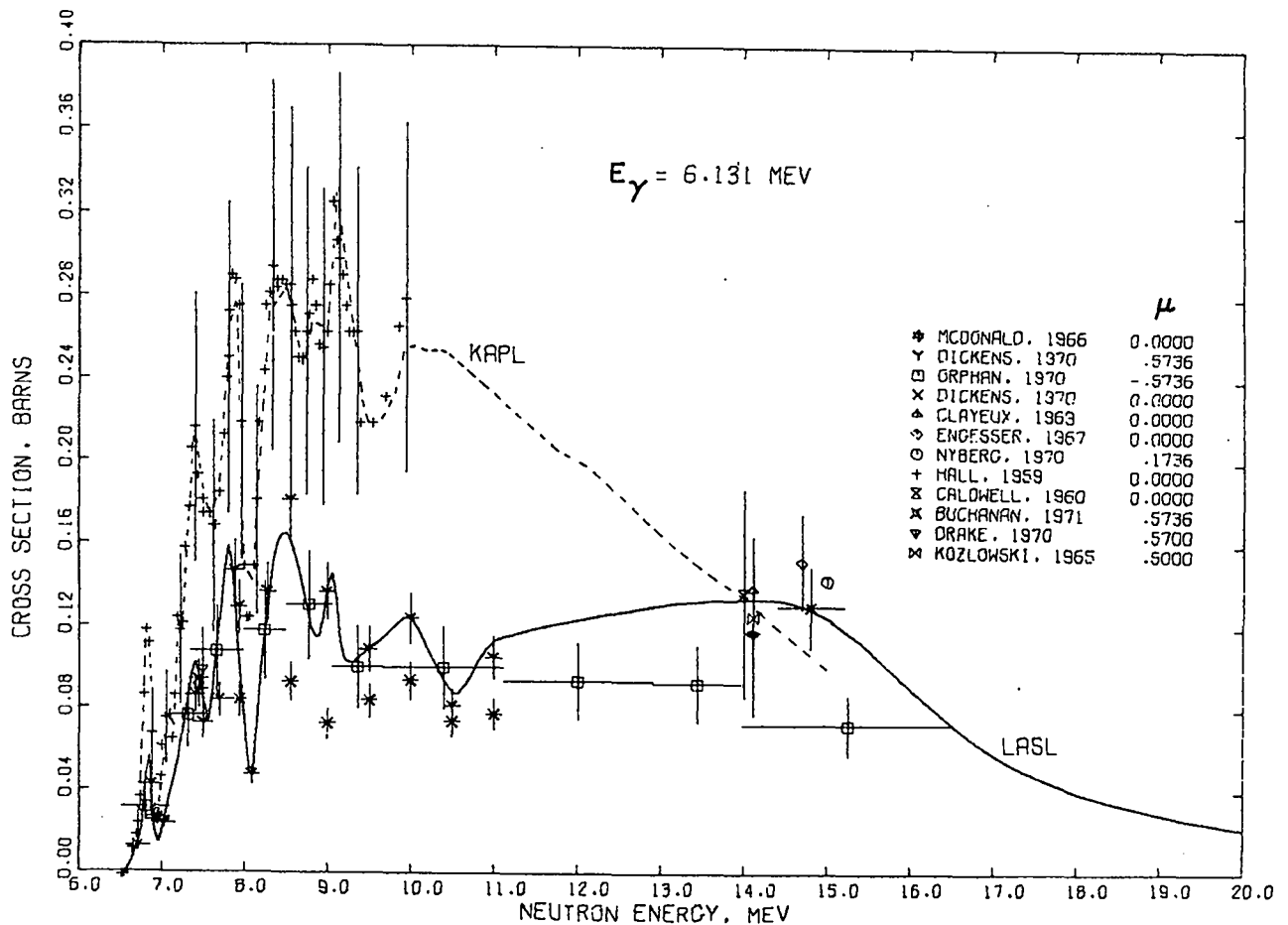


Fig. 10. Measured and evaluated  $(n,n'\gamma)$  cross section for the 6.131-MeV photon.

The evaluated photon-production cross section for the ground-state transition from the 6.131-MeV level is compared in Fig. 10 to the KAPL evaluation\* (S165) and to the available experimental data. All the measurements in Fig. 10 are single-angle ( $\mu = \cos \theta$ ) differential results that have been multiplied by  $4\pi$ . The LASL curve is based mainly on  $55^\circ$  measurements made by Dickens and Perey (Di70) below 11 MeV and on a composite of several measurements near 15 MeV. The single datum at 7.5 MeV by Drake et al. (Dr70) is part of a complete angular-distribution measurement. The Drake data indicate that a significant error ( $\sim 40\%$ ) is introduced at 7.5 MeV by assuming the integrated cross section to be  $4\pi\sigma(55^\circ)$ . This assumption is made throughout the

\* Because photon-production data are not included in the KAPL evaluation, the dashed curve of Fig. 10 was computed from the KAPL  $(n,n')$  cross sections and the decay scheme of Fig. 9.

present evaluation because very few photon angular-distribution measurements exist for oxygen, and we did not perform a detailed theoretical analysis. The differences between the  $55^\circ$  and  $90^\circ$  measurements of Dickens and Perey (Di70) indicate that the anisotropy of the 6.131-MeV photon persists at most neutron energies below 11 MeV. The KAPL curve in Fig. 10 is apparently based on the 1959 measurements of Hall et al. (Ha59) and is roughly a factor of two higher than the LASL curve below 11 MeV.

Similar comparisons are given in Figs. 11 and 12 for the ground-state transitions from the 6.917- and 7.119-MeV levels. Figure 13 includes the photon-production cross sections for the 1.753- and 2.741-MeV photons, both of which result from de-excitation of the 8.872-MeV level in  $^{16}\text{O}$ , and the cross section for the 2.208-MeV photon from the 11.080-MeV level is given in Fig. 14. The KAPL evaluation (S165) is generally higher than our results in Figs. 11-14.

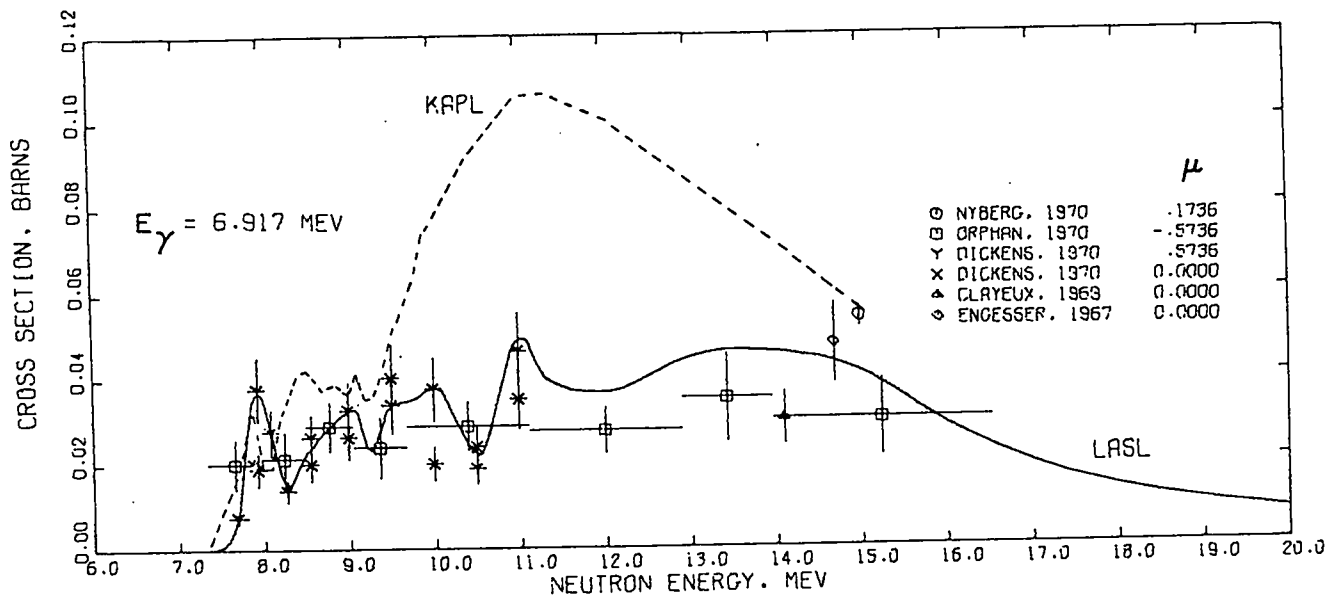


Fig. 11. Measured and evaluated (n,n'γ) cross section for the 6.917-MeV photon.

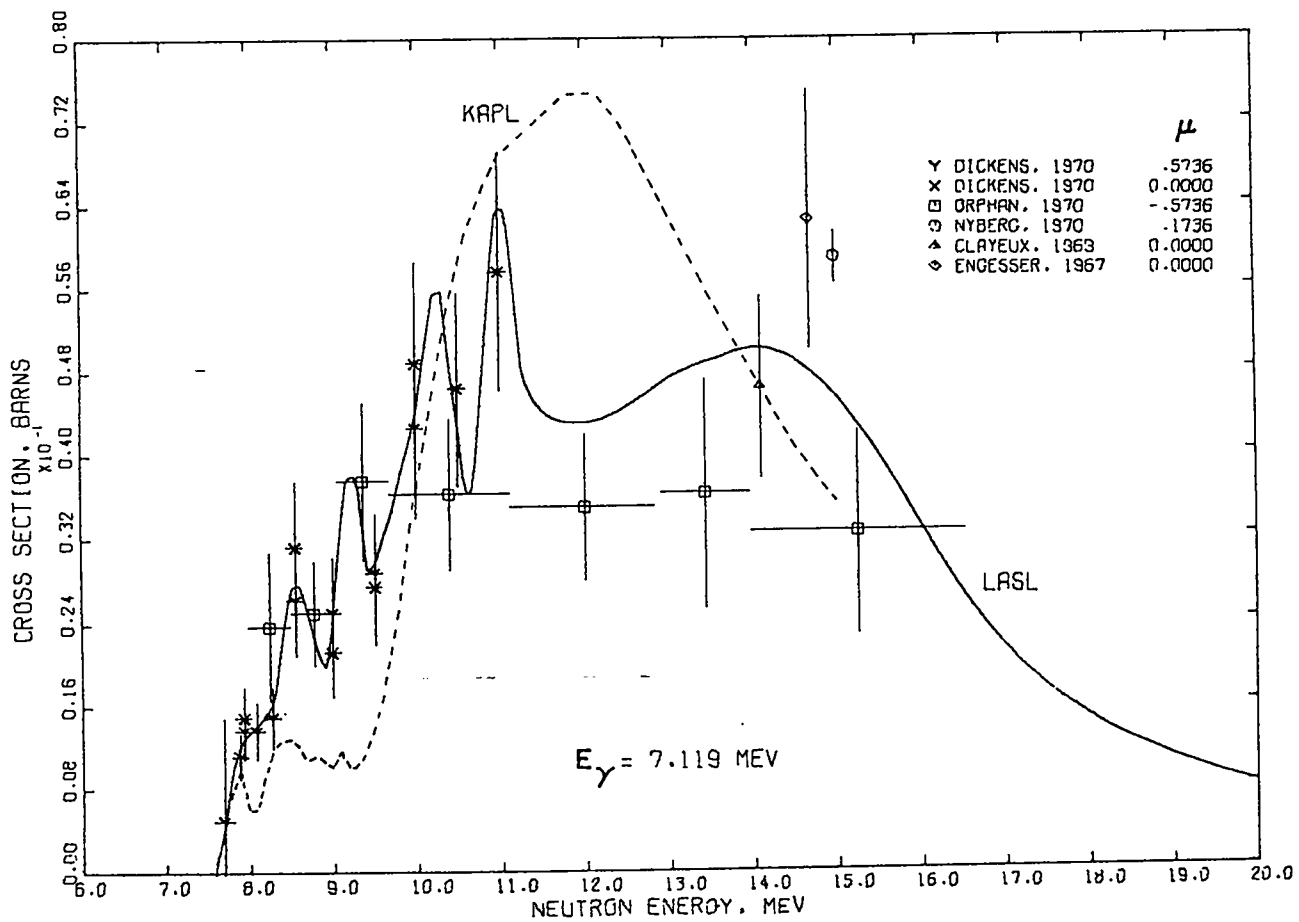


Fig. 12. Measured and evaluated (n,n'γ) cross section for the 7.119-MeV photon.

The 55° and 90° measurements made by Dickens and Perey (Di70) indicate that at most neutron energies the anisotropy in the angular distributions for these photons is significantly less than for the 6.131-MeV photon.

The (n,n') excitation cross sections for the 6.131-, 6.917-, 7.119-, and 8.872-MeV levels that resulted from our analysis of (n,n'γ) measurements are given in Fig. 15. Beyond 15 MeV, the shapes of the curves are taken from compound-nucleus reaction-theory calculations made with the code COMNUC (Du71). The results shown for the 6.052-MeV level also result from COMNUC calculations, normalized with the same factor required to bring the calculated excitation cross sections for the photon-producing levels into approximate agreement with the (n,n'γ) measurements. Similarly, the curves shown in Figs. 15-17 for levels with excitation energy between 8.9 and 13 MeV are based on COMNUC calculations. The normalization for

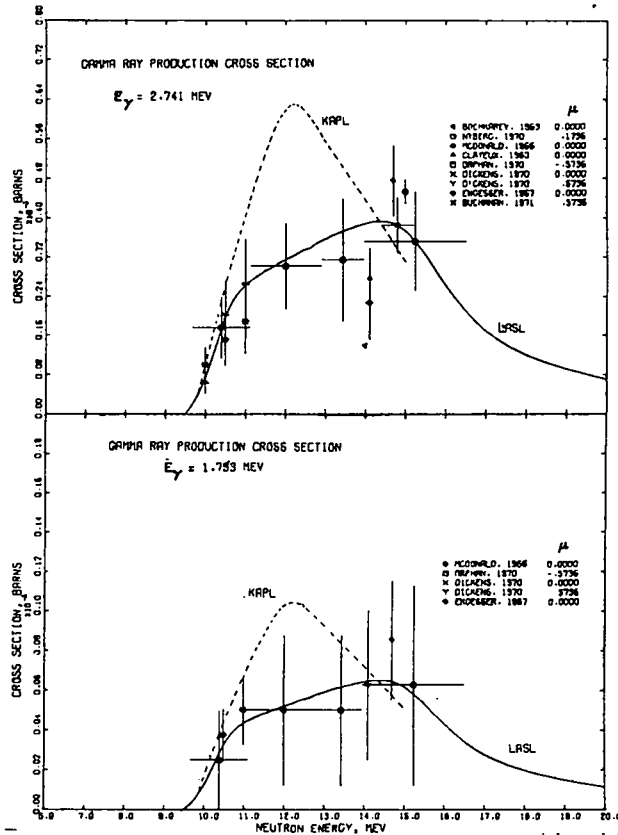


Fig. 13. Measured and evaluated (n,n'γ) cross sections for the 1.753- and 2.741-MeV photons resulting from the 8.872 → 7.119-MeV and 8.872 → 6.131-MeV transitions in  $^{16}\text{O}$ .

these calculations was chosen so that the total cross section minus the reaction cross section near 14 MeV resulted in an elastic cross section consistent with measurements (see Fig. 35 in Sec. 2.7).

The sums of the excitation cross sections for the 6.05- and 6.13-MeV levels and the 6.92- and 7.12-MeV levels are in excellent agreement with direct measurements near 14 MeV made by Bauer et al. (Ba63) and McDonald et al. (Mc66a). The excitation cross section for the 8.87-MeV level deduced from the (n,n'γ) measurements is, however, higher by roughly a factor of 2 than the direct measurement of McDonald et al. (Mc66a).

The total inelastic cross section that results from the above analysis is compared in Fig. 19 to the evaluation of Slaggie and Reynolds (Sl65). The present results are substantially lower than the KAPL curve at energies below 13 MeV, mainly reflecting the difference between the older (n,n'γ) measurements of Hall et al. (Ha59) and the newer measurements of Dickens and Perey (Di70) and Orphan et al. (Or70).

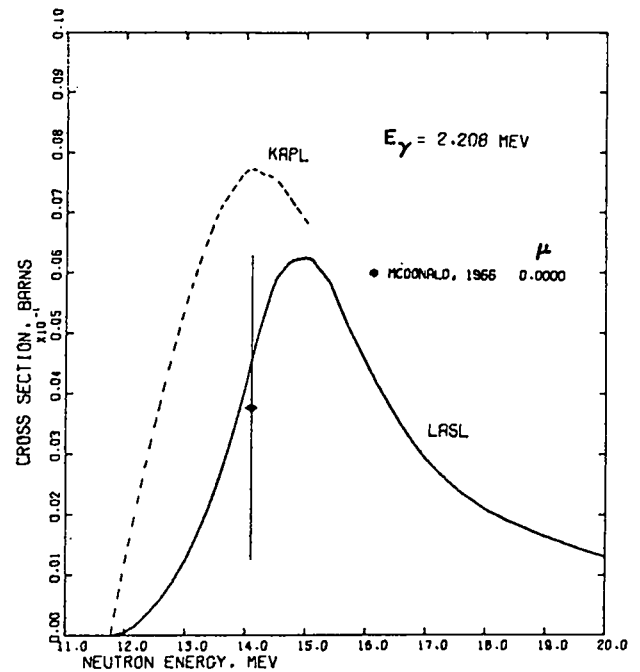


Fig. 14. Measured and evaluated (n,n'γ) cross section for the 2.208-MeV photon resulting from the 11.080 → 8.872-MeV transition in  $^{16}\text{O}$ .

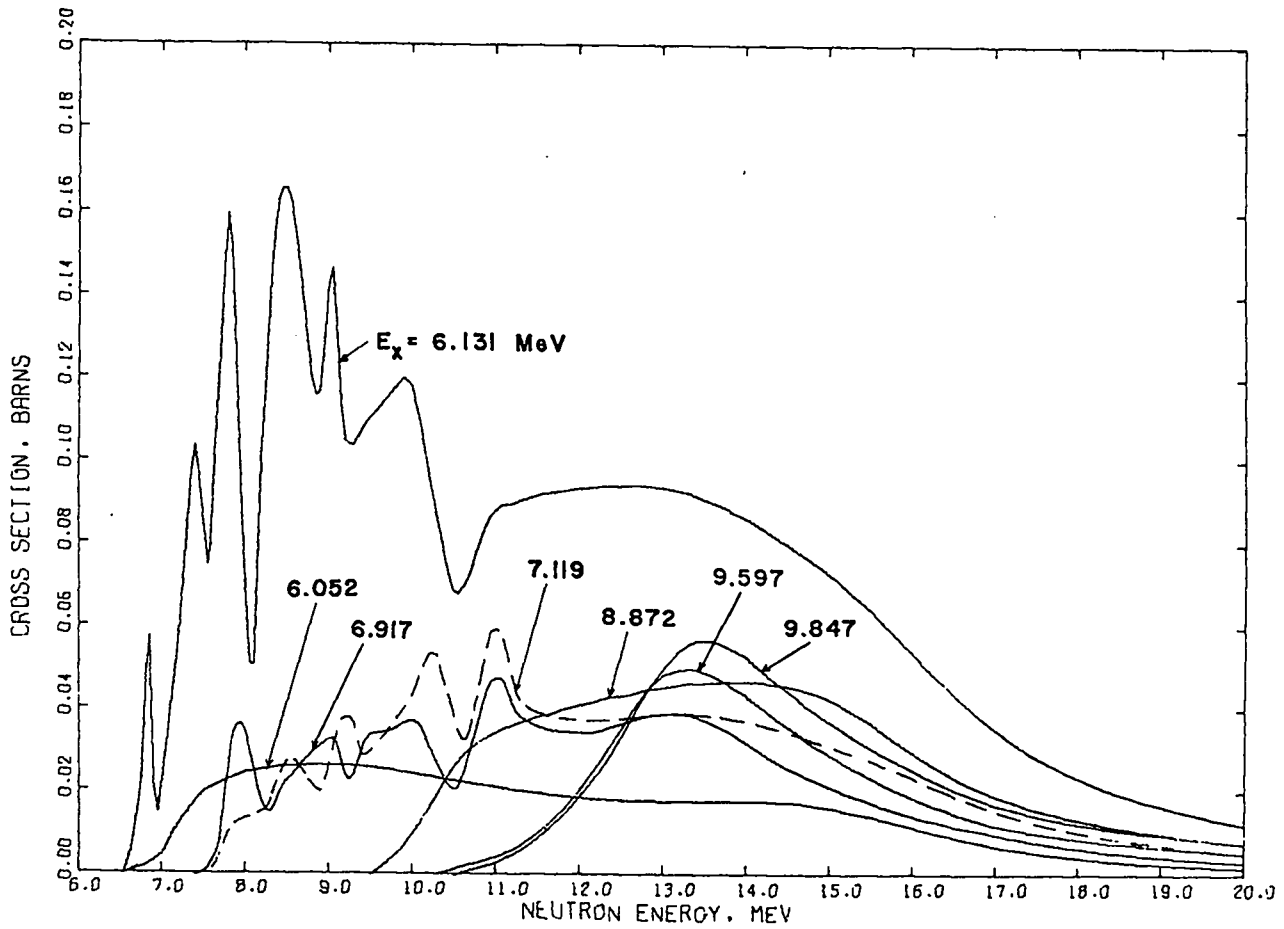


Fig. 15. Evaluated cross sections for inelastic scattering to levels in  $^{16}\text{O}$  with  $E_x < 10$  MeV.

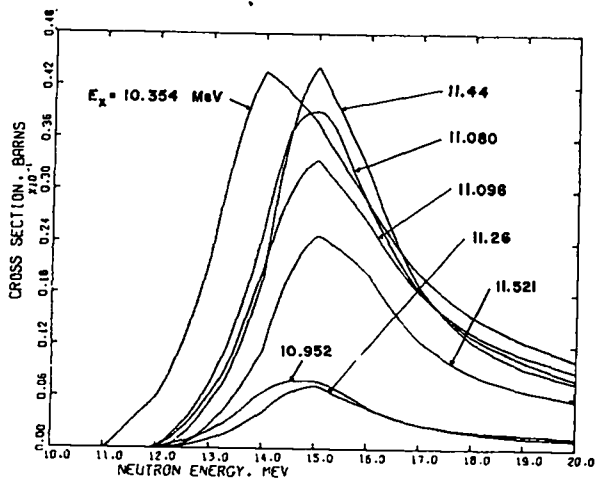


Fig. 16. Evaluated cross sections for inelastic scattering to levels in  $^{16}\text{O}$  with  $E_x$  between 10.354 and 11.521 MeV.

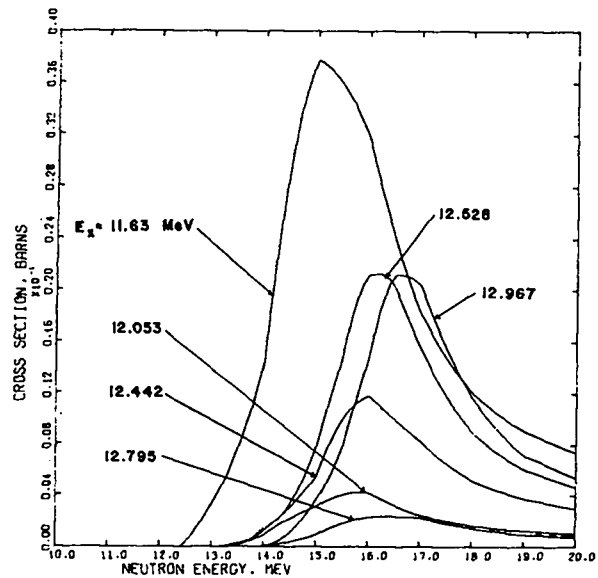


Fig. 17. Evaluated cross sections for inelastic scattering to levels in  $^{16}\text{O}$  with  $E_x$  between 11.63 and 12.967 MeV.

2.3.2. The  $^{16}\text{O}(n,n')$  Cross Section for  $E_x(^{16}\text{O}) > 13$  MeV. At excitation energies above 13 MeV, the level structure in  $^{16}\text{O}$  becomes increasingly less certain, and a simple evaporation model was used to estimate the relative  $(n,n')$  cross section to levels in this region. We used an expression of the form

$$\sigma_{n,n'} \propto (E_0 - E_x) \exp(E_x/T)$$

where  $E_0$  is the total energy available in the center-of-mass system,  $E_x$  is the excitation energy in  $^{16}\text{O}$ , and  $T$  is the nuclear temperature. A value of 2 MeV was used for the temperature. The relative cross sections generated in this manner were normalized so that the nonelastic cross section agreed with the total and elastic cross sections. These results are represented as discrete  $(n,n')$  reactions to 0.3-MeV-wide bands of excitation energy in  $^{16}\text{O}$  and are given in Fig. 18. This representation was used rather than the more usual form of continuous energy spectra to permit more accurate calculation of the effects of center-of-mass motion on the neutron angular distributions (Yo72).

2.4. The  $^{16}\text{O}(n,p)^{16}\text{N}$  and  $^{16}\text{O}(n,\text{py})^{16}\text{N}$  Cross Sections

The evaluated  $(n,p)$  cross section of Slaggie and Reynolds (Sl65) below 15 MeV was adopted in the present study. From 15 to 17 MeV, we used experimental data to determine the  $(n,p)$  cross section, and above 17 MeV we joined a shape calculated with the code COMNUC to the lower-energy results. The evaluated curve is compared to the available measurements in Fig. 20. Most of the high energy

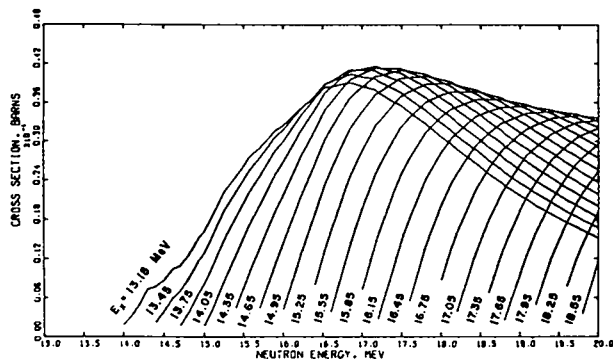


Fig. 18. Evaluated  $(n,n')$  cross sections to groups of levels in  $^{16}\text{O}$  with  $E_x$  between 15 and 19 MeV. Each 0.3 MeV in excitation energy is represented as a single fictitious level at the midpoint energy.

measurements (e.g., Bo67, De60, De62, Ka62, Ma54, Mi66, Pa53, Pr66, Se62) result from activation studies; the evaluated curve therefore does not include  $(n,p)$  reactions to particle-unstable states\* of  $^{16}\text{N}$ .

Several low-energy photons are produced by the  $^{16}\text{O}(n,\text{py})^{16}\text{N}$  reaction, as indicated in the  $^{16}\text{N}$  level decay scheme of Fig. 21. No experimental data are available on these transitions, and the individual  $(n,p)$  level excitation cross sections are not included explicitly in the evaluation. We estimated the  $(n,\text{py})$  cross sections, however, by distributing the evaluated  $(n,p)$  cross section of Fig. 20 among the particle-stable states of  $^{16}\text{N}$ , assuming the population of each to be proportional to  $(2J+1)$ . Table III gives a summary of the  $(n,\text{py})$  transitions included in the evaluation. Two of the transitions have been combined, as indicated.

TABLE III  
GAMMA RAYS FROM  
 $^{16}\text{O}(n,\text{py})^{16}\text{N}$  REACTIONS

$E_\gamma$ (MeV)	$E_{\text{initial}}$ (MeV)	$E_{\text{final}}$ (MeV)
0.397	0.397	0
0.292	0.297	0
	0.397	0.121
0.120	0.121	0
	0.397	0.297

\* In this context we exclude beta emission in defining "particle-stable" levels.

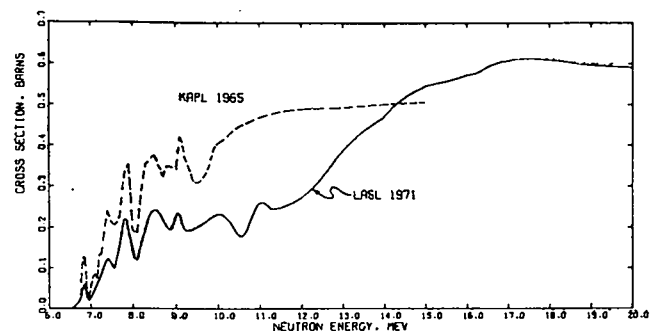


Fig. 19. Evaluated total inelastic cross section from 6 to 20 MeV. The LASL curve includes  $(n,n'\alpha)$  and  $(n,n'p)$  contributions.

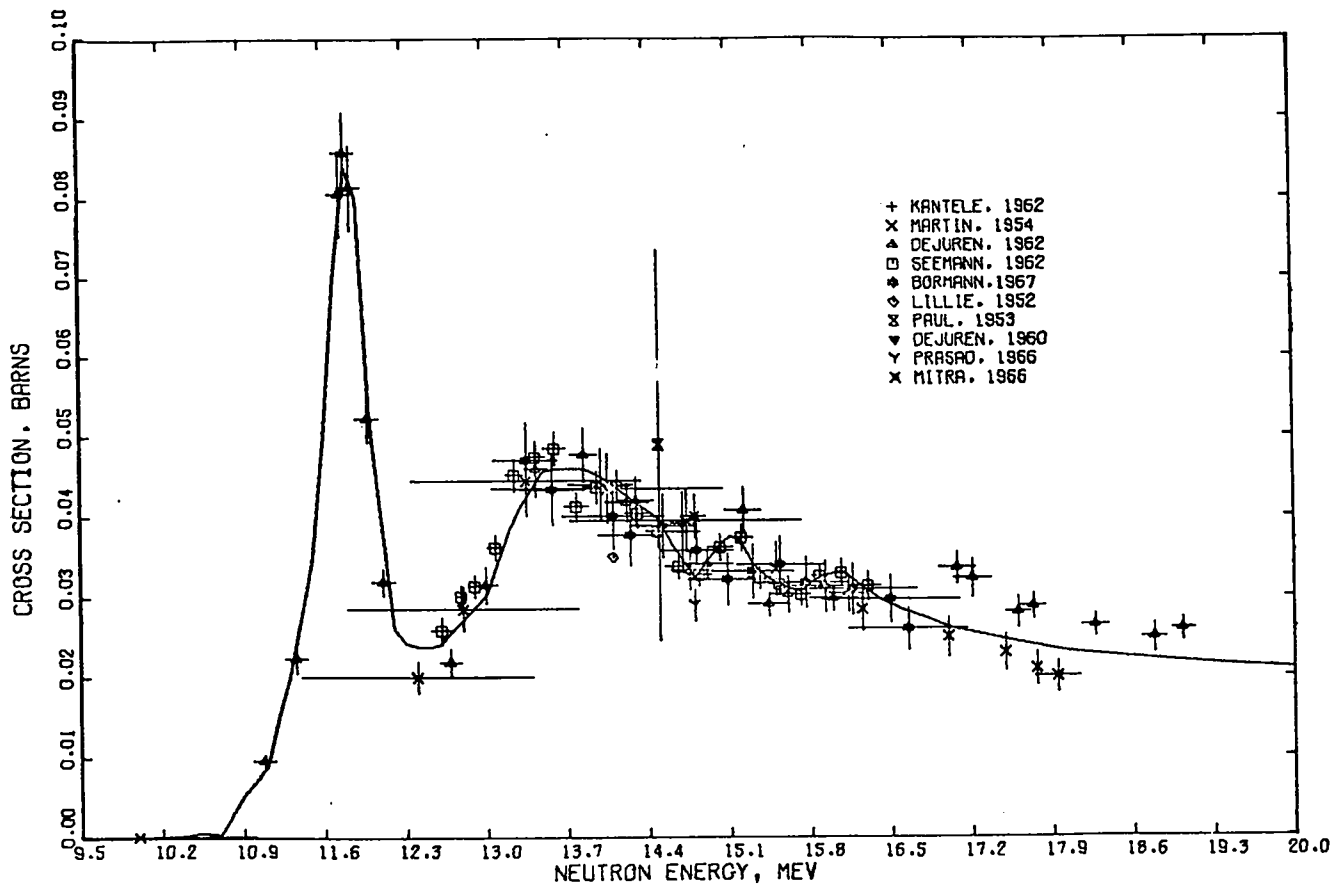


Fig. 20. Measured and evaluated total (n,p) cross section for  $^{16}\text{O}$  from 10 to 20 MeV.

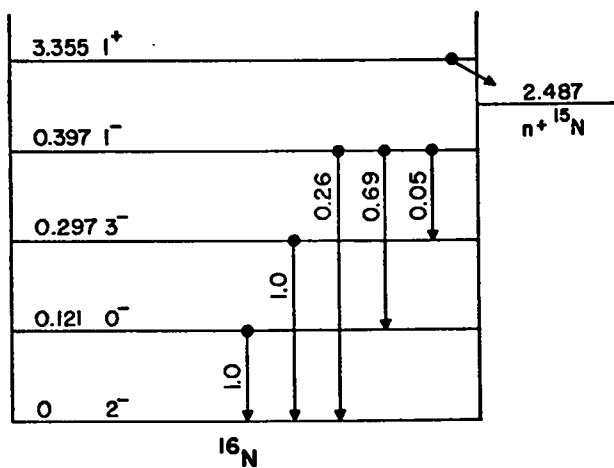


Fig. 21. Energy-level decay scheme for  $^{16}\text{N}$ .

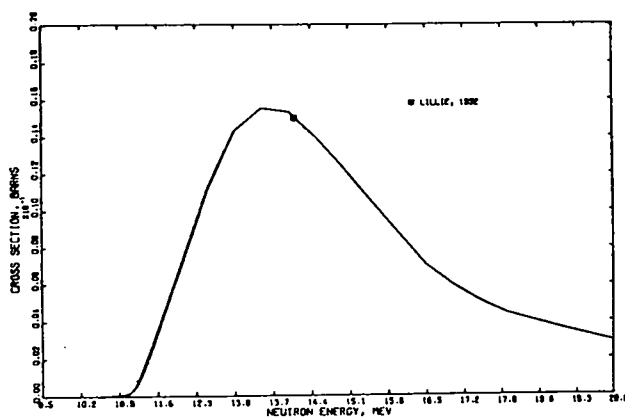


Fig. 22. Measured and evaluated total (n,d) cross section for  $^{16}\text{O}$  from 10 to 20 MeV.

2.5. The  $^{16}\text{O}(n,d)^{15}\text{N}$  Cross Section

The (n,d) cross section is given in Fig. 22. The evaluated curve is based on a compound-nucleus reaction-theory calculation with the code COMNUC, normalized to the lone measurement by Lillie (L152) near 14 MeV. Because the threshold for the (n,d) reaction does not occur until 16.1 MeV, photon production from (n,d) reactions was ignored.

2.6. The  $^{16}\text{O}(n,\alpha)^{13}\text{C}$  and  $^{16}\text{O}(n,\alpha\gamma)^{13}\text{C}$  Cross Sections.

At excitation energies higher than 4.947 MeV,  $^{13}\text{C}$  levels decay predominantly by neutron emission, as indicated in the decay scheme of Fig. 23. The excitation cross sections to the ground and first three excited states are included in the present evaluation, and the sum of these is given as the total (n, $\alpha$ ) cross section. The (n, $\alpha n$ ) cross section through the higher levels is lumped with the (n,n' $\alpha$ ) cross section discussed in Sec. 2.3.2. The photon transitions included in this study are given in Table IV.

Figure 24 shows the (n, $\alpha_0$ ) cross section from threshold to 6 MeV. The Slaggie and Reynolds (S165) evaluation was adopted in this region, and the

TABLE IV  
GAMMA RAYS FROM  
 $^{16}\text{O}(n,\alpha\gamma)^{13}\text{C}$  REACTIONS

$E_\gamma$ (MeV)	$E_{\text{initial}}$ (MeV)	$E_{\text{final}}$ (MeV)
3.854	3.854	0
3.684	3.684	0
3.086	3.086	0
0.683	{ 3.854 3.684	{ 3.086 3.086
0.170	3.854	3.684

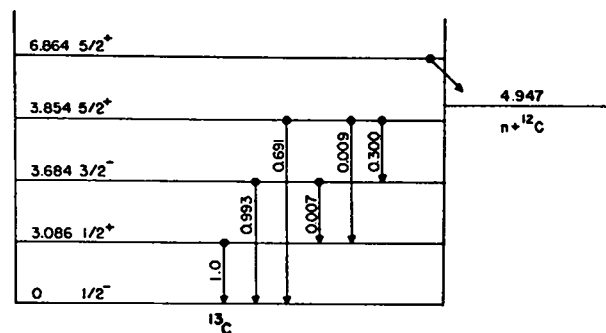


Fig. 23. Energy-level decay scheme for  $^{13}\text{C}$ .

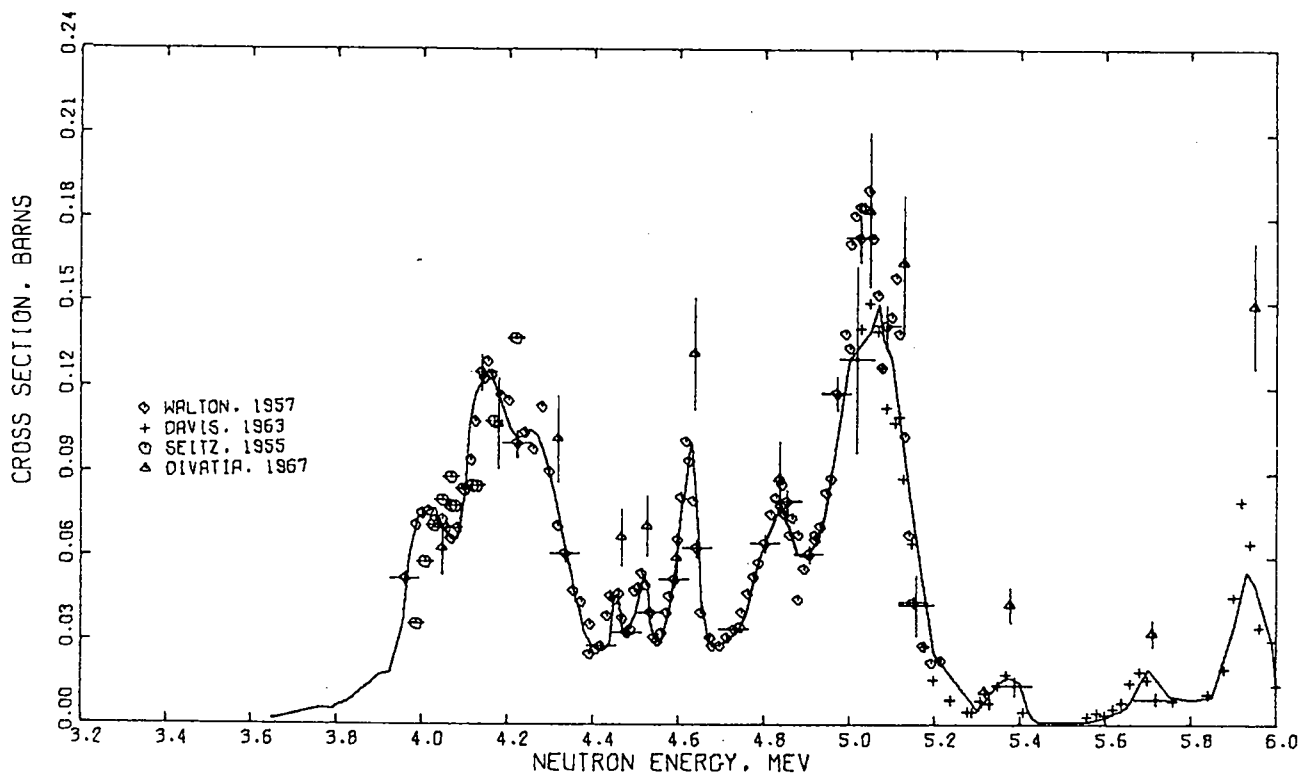


Fig. 24. Measured and evaluated (n, $\alpha_0$ ) cross section between 3.2 and 6.0 MeV.

agreement with the available measurements is reasonable. Above 6 MeV, we reevaluated the  $(n, \alpha_0)$  reaction, and the results are compared to experiment in Fig. 25. At higher energies the curve is based mainly on the measurements of Sick et al. (Si68).

The  $(n, \alpha_1)$  cross section below 15 MeV was determined from measurements of the direct  $(n, \alpha_1)$  cross section to the 3.086-MeV level and from measurements of the ground-state photon transition from that level, as given in Fig. 26. The excitation cross sections to the 3.684- and 3.854-MeV levels are based on measurements of the ground-state photons below 15 MeV, using the decay scheme shown in Fig. 23, and the resulting photon-production cross sections are given in Figs. 27 and 28. At energies above 15 MeV, we obtained the  $(n, \alpha)$  cross sections to the first three excited levels by dividing the total  $(n, \alpha)$  cross section available to these levels, as measured by Sick et al. (Si68) and shown in Fig. 29, among the three states assuming each is populated in the same ratio as occurs near 15 MeV.

The total  $(n, \alpha)$  cross section is given by the solid curve in Fig. 30. The experimental results in the figure are actually measurements of the alpha-emission cross section, and the rapid increase in the measurements above 12 MeV is caused by the onset of the  $(n, n'\alpha)$  reaction. The difference between the

KAPL and LASL  $(n, \alpha)$  curves occurs because part of the  $(n, n'\alpha)$  cross section was apparently included in the KAPL curve, whereas we chose to include that reaction in our  $(n, n')$  files, designating alpha emission as the mode of decay of the residual nucleus.

The total alpha-emission cross section constructed from our  $(n, n'\alpha)$  and  $(n, \alpha)$  cross sections is also given in Fig. 30. At all energies above 13 MeV, our results are higher than the experimental data. It should be noted, however, that the low-energy portion of the alpha spectrum is difficult to measure accurately, so the agreement is probably reasonable below 17 MeV. Above 17 MeV, however, the evaluated curve is too high, probably because proton decay following  $(n, n')$  reactions [i.e., the  $(n, n'p)$  reaction] is competing more effectively with alpha decay than we have assumed. This problem was not discovered until the evaluation had been completed. The cross section for proton emission, corresponding to the sum of the total  $(n, p)$  and  $(n, n'p)$  reactions, is given in Fig. 31, together with the alpha-emission cross section\* and the total  $(n, n')$  cross section to gamma-decaying levels. A slight increase in the  $(n, n'p)$  cross section with a corresponding decrease in  $(n, n'\alpha)$  would correct the problem above 17 MeV in Fig. 30.

\*The structure in the alpha-emission cross section above 15 MeV in Fig. 31 is artificial and results from the particular representation that we used in the ENDF/B files.

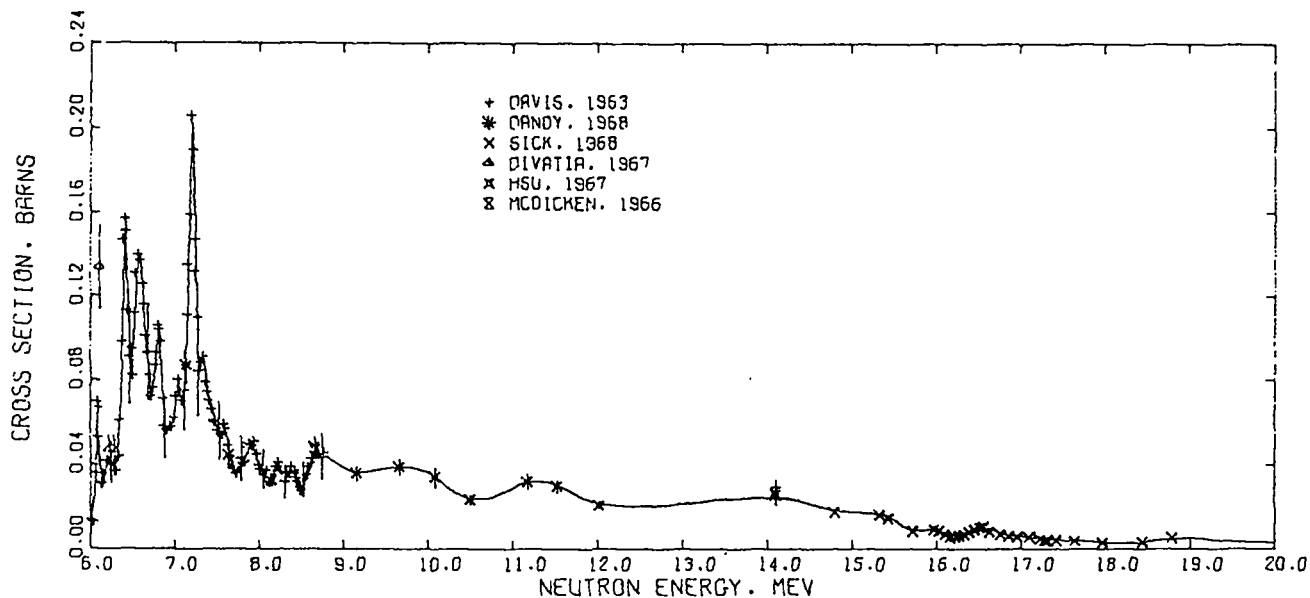


Fig. 25. Measured and evaluated  $(n, \alpha_0)$  cross section between 6 and 20 MeV.

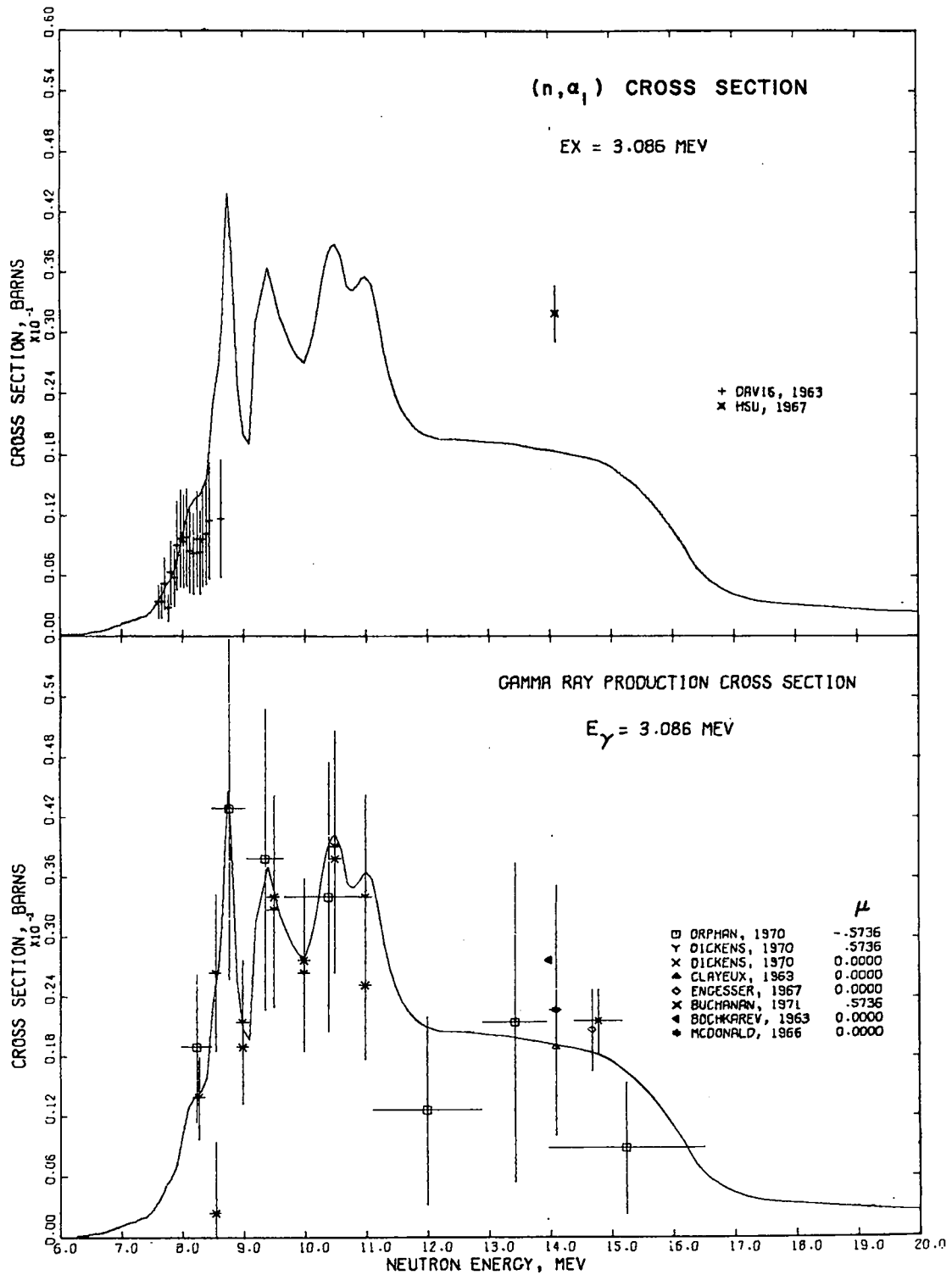


Fig. 26. Measured and evaluated  $(n, \alpha_1)$  and  $(n, \alpha\gamma)$  cross sections for the 3.086-MeV level and ground-state transition in  $^{13}\text{C}$ .

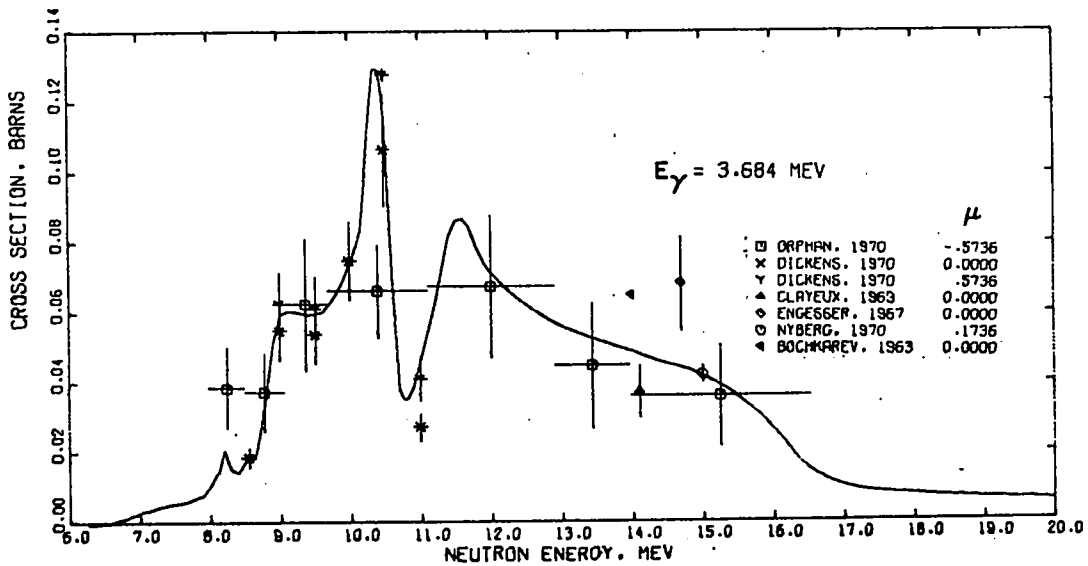


Fig. 27. Measured and evaluated (n,α) cross section for the 3.684-MeV photon.

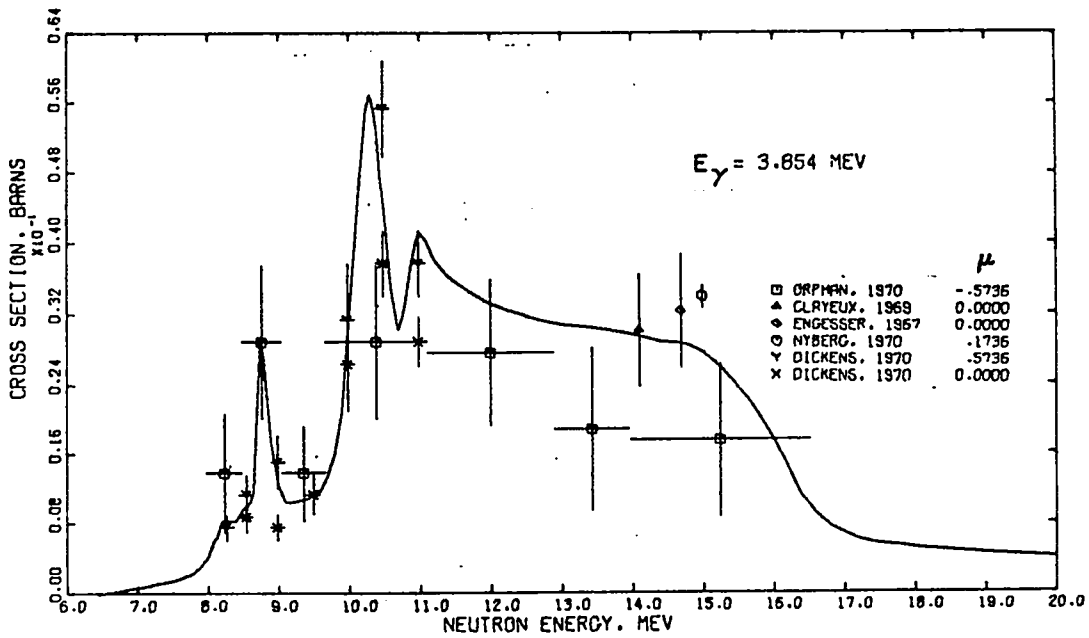


Fig. 28. Measured and evaluated (n,α) cross section for the 3.854-MeV photon.

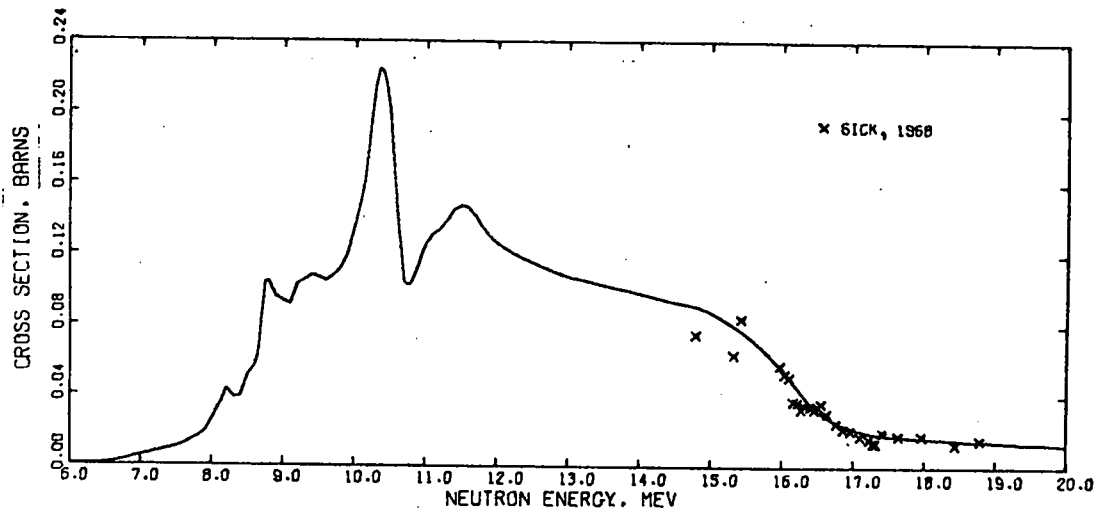


Fig. 29. Measured and evaluated composite (n,α) cross section to the first three excited levels of  $^{13}\text{C}$ .

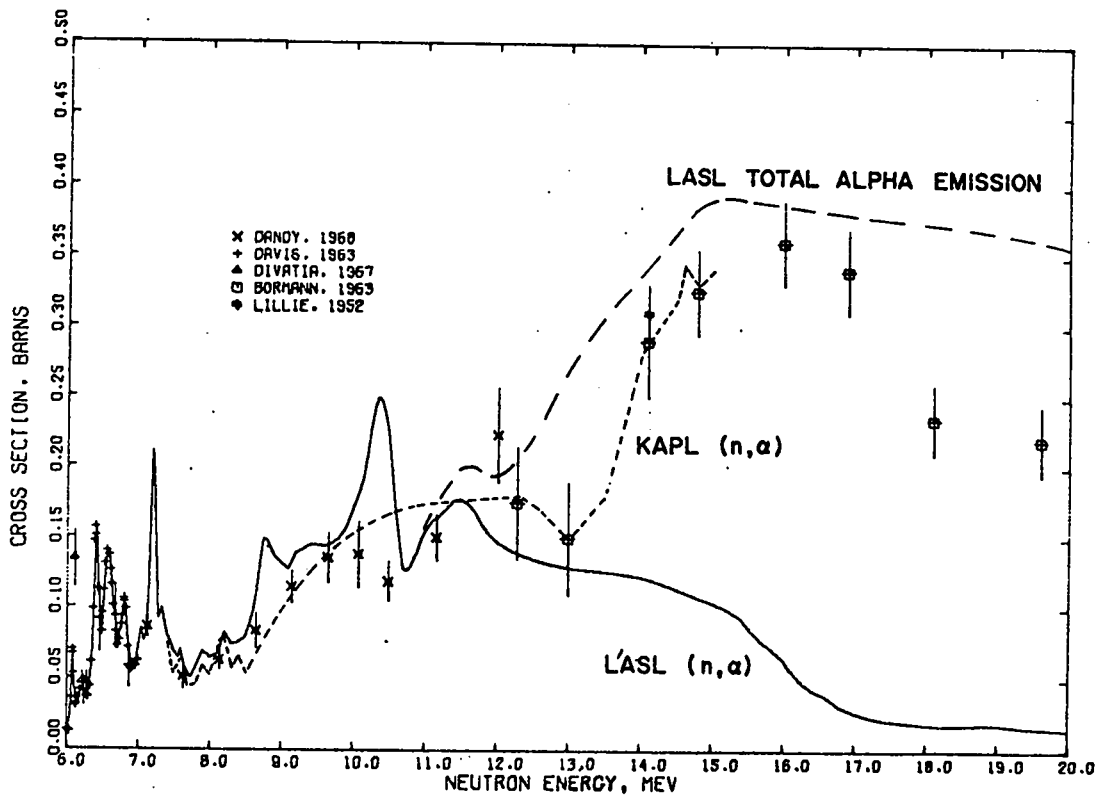


Fig. 30. Measured and evaluated total alpha emission cross section compared to the LASL and KAPL (n,α) evaluations.

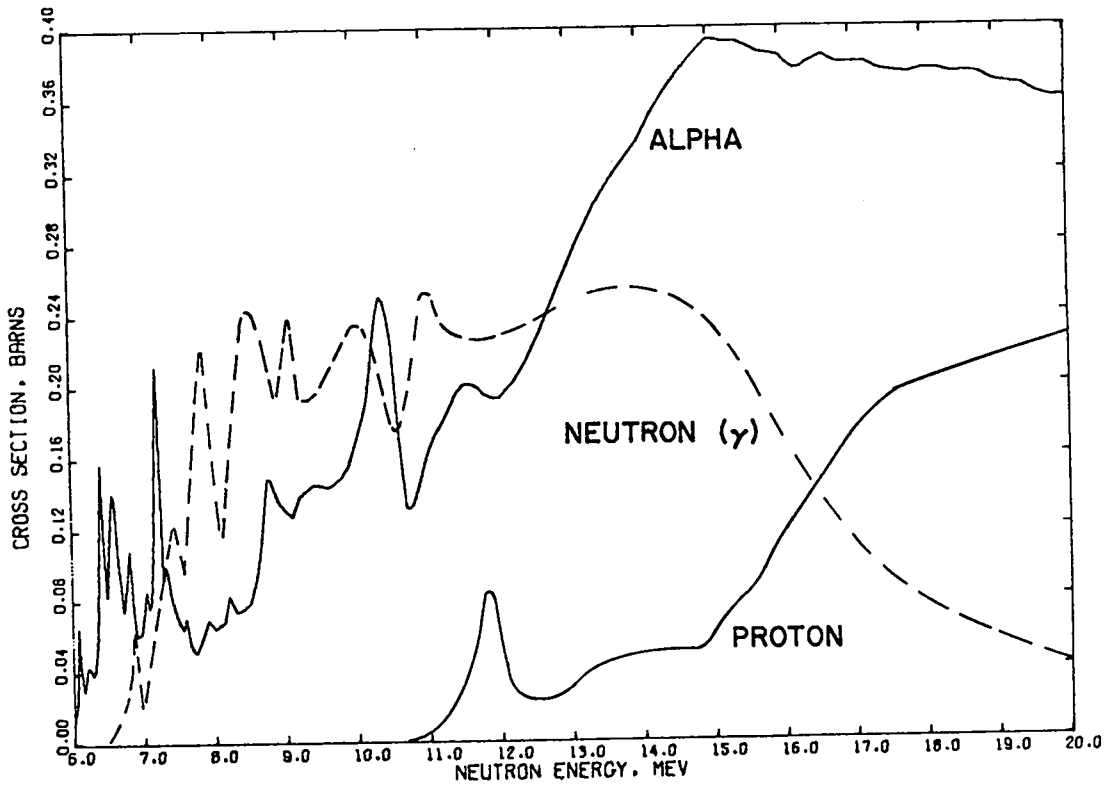


Fig. 31. The total alpha and proton emission cross sections compared to the portion of the inelastic neutron cross section that results in photon emission.

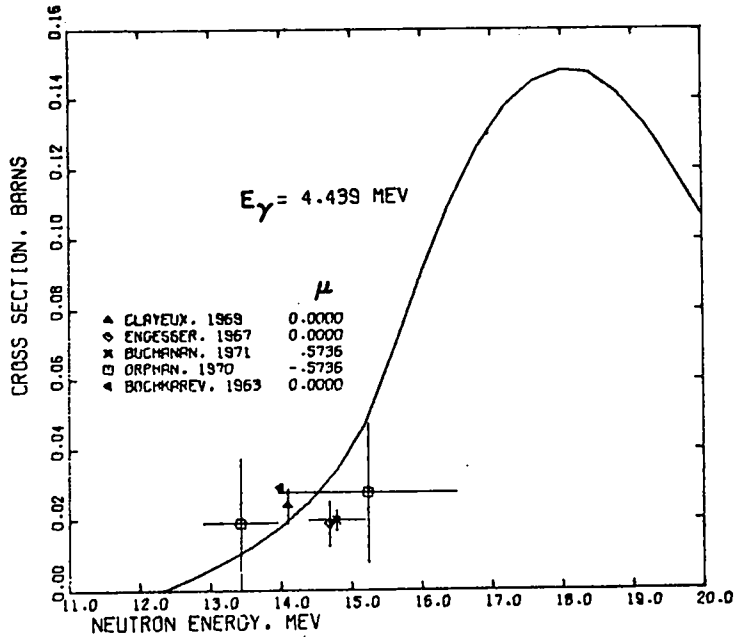


Fig. 32. Measured and evaluated  $(n, n'\alpha\gamma)$  cross section for the 4.439-MeV photon.

A significant portion of the  $(n,n'\alpha)$  cross section results in excitation of the first excited level at 4.439 MeV in  $^{12}\text{C}$ , with subsequent emission of a photon of that energy. We made a crude estimate of the  $(n,n'\alpha\gamma)$  cross section from the  $(n,n'\alpha)$  data using a technique described earlier (Yo72), and the results are compared to the available photon-production measurements in Fig. 32. The threshold for photon production following  $(n,n'p)$  reactions does not occur until 18.49 MeV, and we have ignored photons from this reaction in this study.

### 2.7. Elastic Scattering Cross Section

Although the threshold for the  $(n,\alpha)$  reaction is 2.35 MeV, this channel does not become important until nearly 4 MeV, and at lower energies the elastic cross section is essentially equal to the total cross section. The elastic cross section obtained from our analysis of the total is compared in Fig. 33 to the available elastic measurements between 0 and

2.8 MeV. Similarly, Fig. 34 includes the elastic results between 2.8 and 6.0 MeV. Above 4 MeV, the  $(n,\alpha)$  cross section has been subtracted from the total to give the elastic curve. Clearly, the elastic measurements shown in Figs. 33 and 34 are in reasonable agreement with the evaluated curve, although the measurements do not show much of the structure displayed by the total cross section. Below 6 MeV, the Slaggie and Reynolds (Sl65) elastic data are only slightly different from the present results, and the only important difference occurs in the window near 2.35 MeV, as noted in Sec. 2.1.

The elastic cross section from 6 to 20 MeV is given in Fig. 35. The KAPL elastic (Sl65) is included for comparison. Most of the experimental points in Fig. 35 were obtained by fitting the measured angular distributions with Legendre expansions. The fitted curves above 7 MeV were anchored at front and back angles by inserting into the fit fictitious

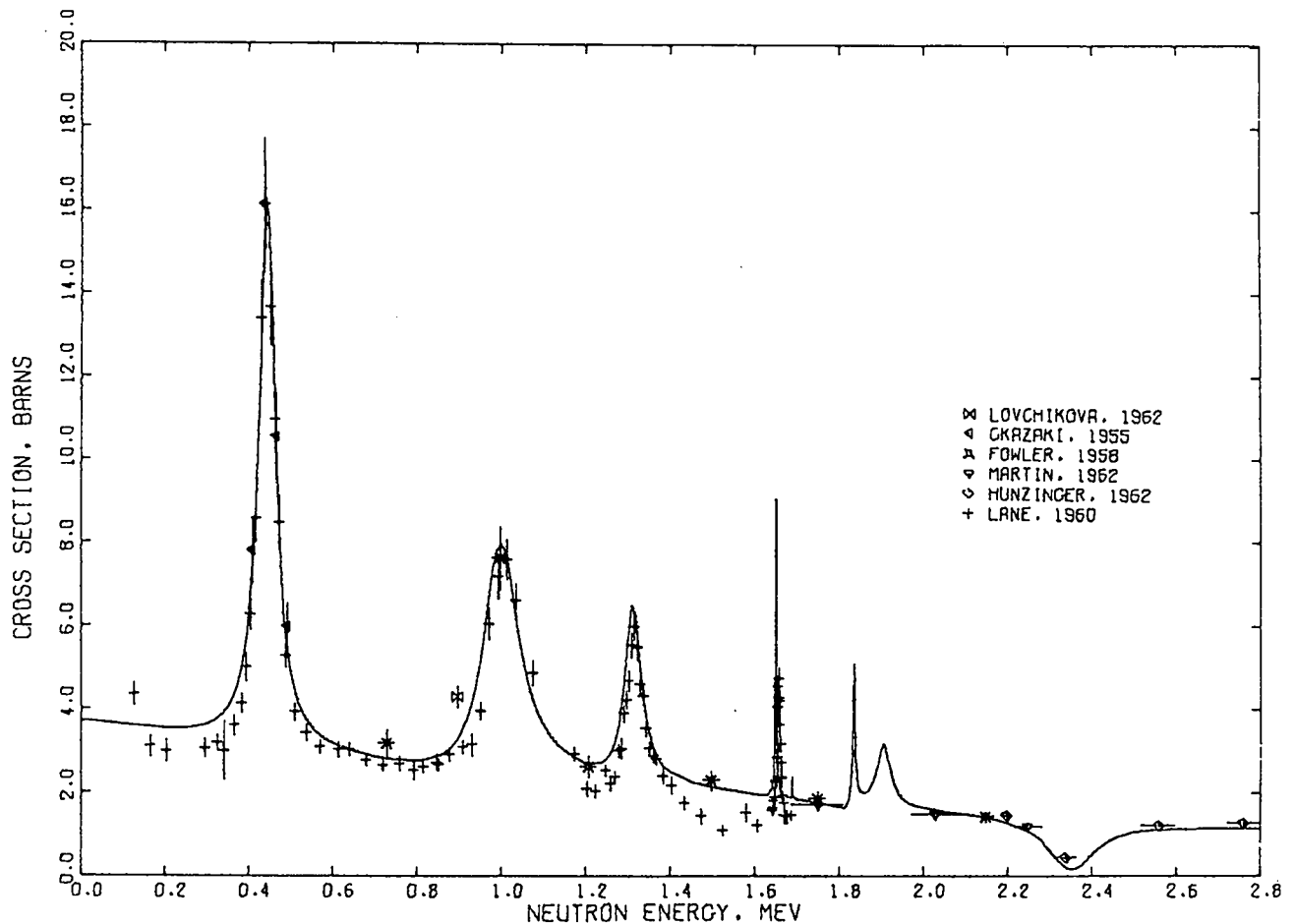


Fig. 33. Measured and evaluated elastic scattering cross section for  $^{12}\text{C}$  from 0 to 2.8 MeV.

points at  $0^\circ$  based on Wick's limit (W143) and points at back angles based on optical model calculations.

The evaluated curve below 11 MeV was obtained by subtracting the sum of all reaction cross sections from the total cross section. Between 11 and 14 MeV the emphasis was shifted to the elastic measurements, and near 14 MeV the elastic was obtained directly from experimental data. To extend the elastic cross section to higher energies, the parameters of a spherical optical model were fitted to the angular distribution measurements near 14 MeV. The depth of the real potential was then varied to reproduce the total cross section to 20 MeV, and the elastic cross section was obtained by subtracting from the fluctuating total cross section a smooth nonelastic cross section based on the calculations.

The evaluated elastic cross section is in good agreement with most of the measurements in Fig. 35, although the curve is somewhat higher than the measurements near 11 and 11.6 MeV. Above 9 MeV, the evaluated curve is substantially higher than the KAPL results (S165). The 1953 cloud chamber measurement by Conner (Co53), which roughly agrees with the KAPL data, was not emphasized in the present study.

### 3. ANGULAR DISTRIBUTIONS

#### 3.1. Elastic Neutron Angular Distributions

The evaluated angular distributions for elastic scattering by Slaggie and Reynolds (S165) were adopted for neutron energies below 5 MeV. From 5 to 14 MeV smooth curves were drawn through the coefficients obtained from Legendre fits to the available experimental data. Above 7 MeV the fits were anchored at front and back angles using Wick's limit (W143) and optical model calculations, as noted earlier. Above 14 MeV the behavior of the Legendre coefficients was estimated from the optical model calculations that were used to extrapolate the elastic cross section to 20 MeV (Sec. 2.7).

In Fig. 36 the evaluated Legendre coefficients\* for  $l = 1$  through  $l = 4$  are compared to the fitted values for neutron energies above 5 MeV. Similarly, the coefficients for  $l = 5$  through  $l = 10$  are given in Fig. 37. Near 11 MeV there are significant differences in the  $l = 7$  and  $l = 8$  coefficients from

\*These coefficients are in the ENDF form defined

$$\text{by } \sigma(\theta) = \frac{\sigma_{\text{int}}}{4\pi} \sum_{l=0}^{2L} (2l+1) f_l P_l(\cos \theta), \text{ with } f_0=1 \text{ and } |f_l| \leq 1.$$

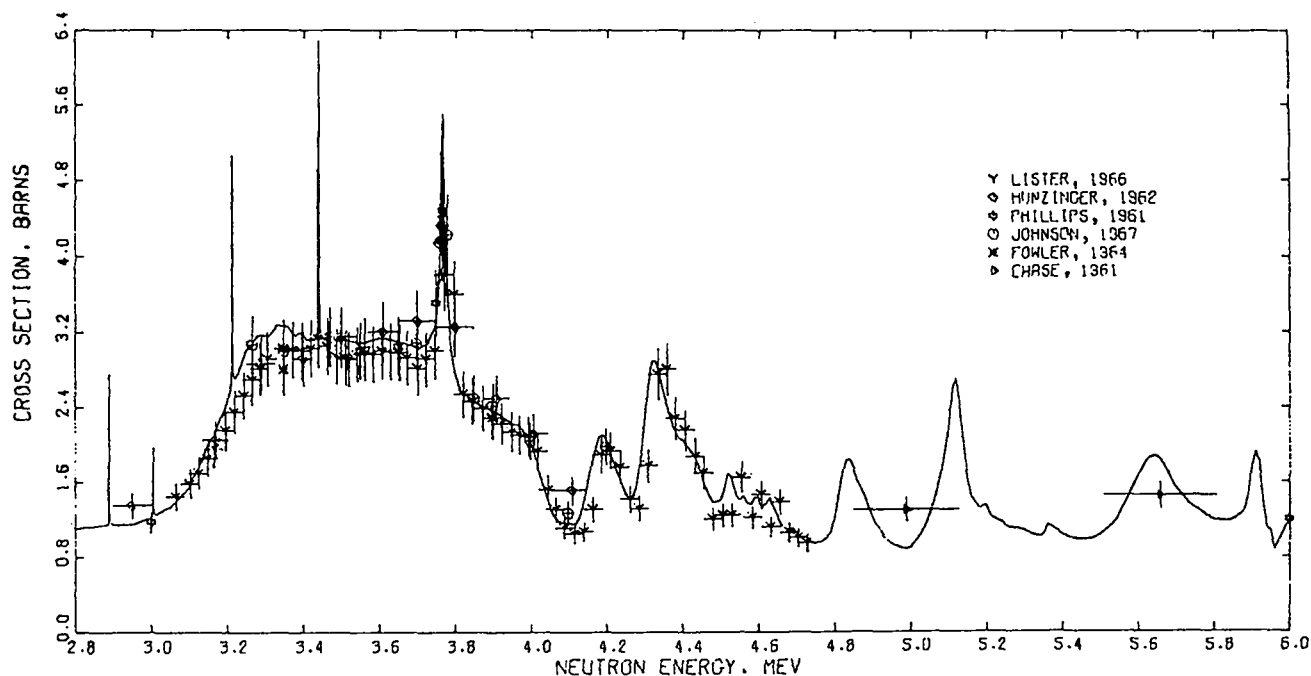


Fig. 34. Measured and evaluated elastic scattering cross section for  $^{16}\text{O}$  from 2.8 to 6.0 MeV.

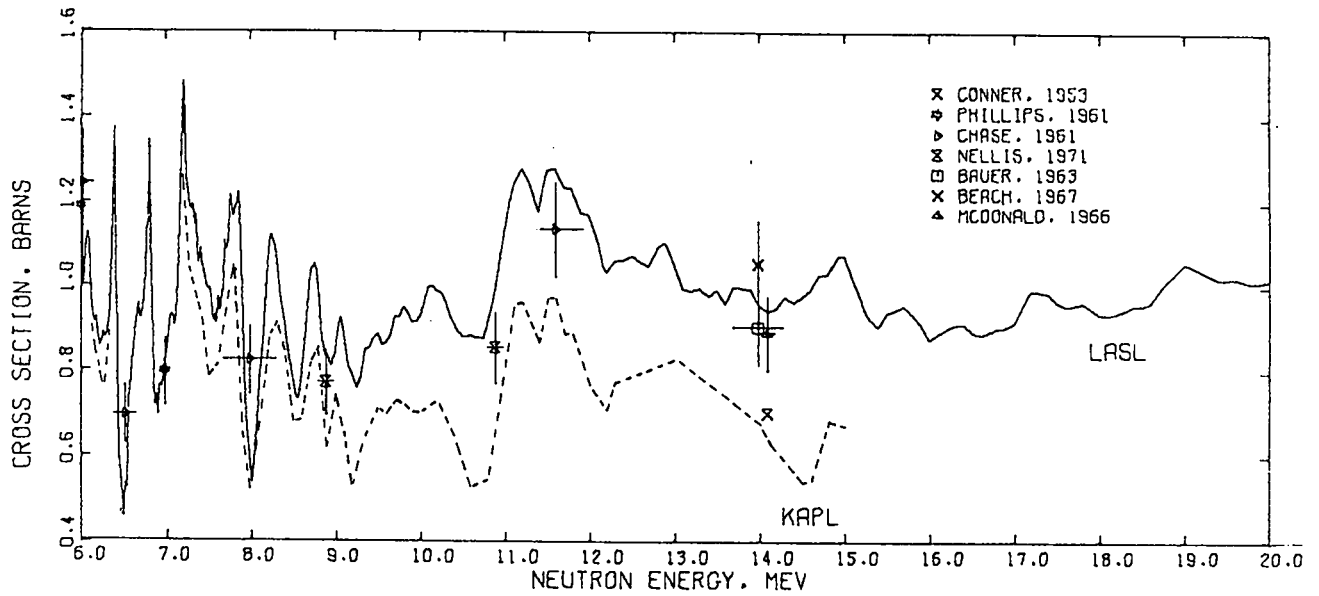


Fig. 35. Measured and evaluated elastic scattering cross section for  $^{16}\text{O}$  from 6 to 20 MeV.

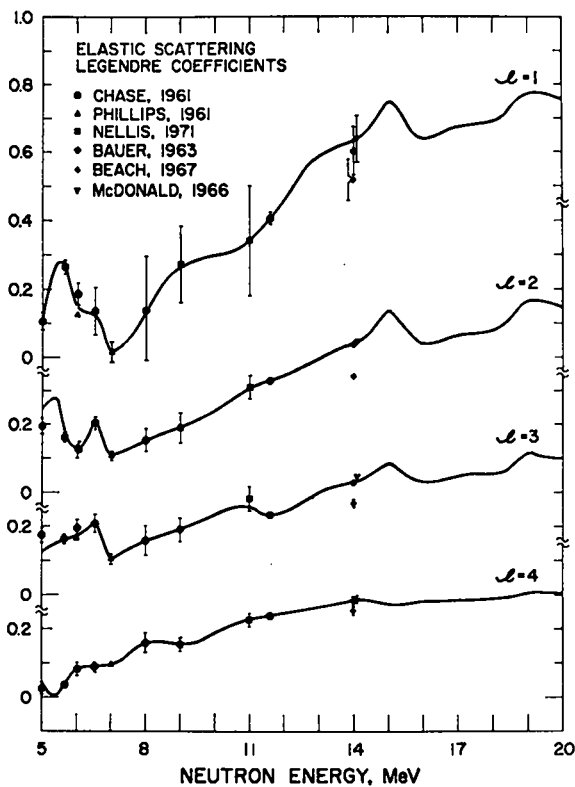


Fig. 36. Measured and evaluated Legendre coefficients for  $l = 1$  through  $l = 4$  at neutron energies above 5 MeV. The ENDF/B convention is used for the coefficients ( $f \equiv 1$ ).

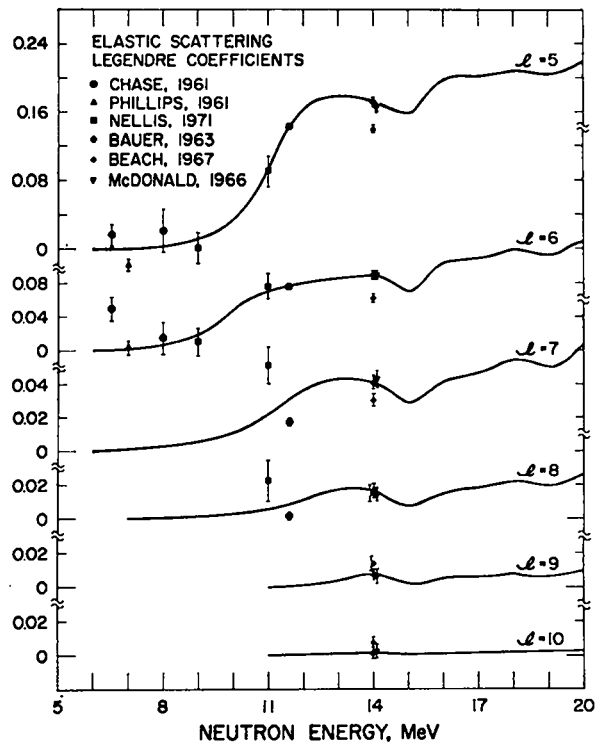


Fig. 37. Measured and evaluated Legendre coefficients for  $l = 5$  through  $l = 10$  at neutron energies above 5 MeV.

the Nellis et al. (Ne71) and the Chase et al. (Ch61) measurements. While these differences may be real because there is structure in the total cross section near 11 MeV, we used average values for the coefficients in this analysis. Significant differences also occur in the coefficients from the Beach (Be67) data as compared to those from the Bauer et al. (Ba63) and McDonald et al. (Mc66a) measurements near 14 MeV. The results from the latter experiments were used in this analysis.

The elastic angular distributions are compared in Fig. 38 to the measurements between 4.99 and 6.53 MeV. Similar comparisons are given in Figs. 39 and 40 for the elastic measurements between 7 and 14.1 MeV. The values used in the figures for Wick's limit were averaged roughly over the energy resolution of the experimental measurements. The differences noted earlier between the Nellis (Ne71) and Chase (Ch61) measurements near 11 MeV are apparent in Fig. 39. Similarly, in Fig. 40 the evaluated

curve at 14.1 MeV differs significantly from the Beach (Be67) measurement.

Angular distributions obtained from the optical model calculations are given in Fig. 41 for neutron energies of 16, 18, and 20 MeV. The distributions become progressively more forward-peaked as the neutron energy increases.

### 3.2. Inelastic Neutron Angular Distributions

Measurements of inelastic neutron angular distributions for some of the low-lying levels of  $^{16}\text{O}$  have been made at 9 and 11 MeV by Nellis et al. (Ne71) and near 14 MeV by Bauer et al. (Ba63) and McDonald et al. (Mc66a). The Nellis data indicate that the sum of the angular distributions to the 6.05- and 6.13-MeV levels is somewhat forward-peaked at 9 and 11 MeV, and similar effects are observed in the measurements near 14 MeV (Ba63, Mc66a). The sum of the angular distributions to the 6.92- and 7.12-MeV levels is nearly isotropic at 11 MeV (Ne71),

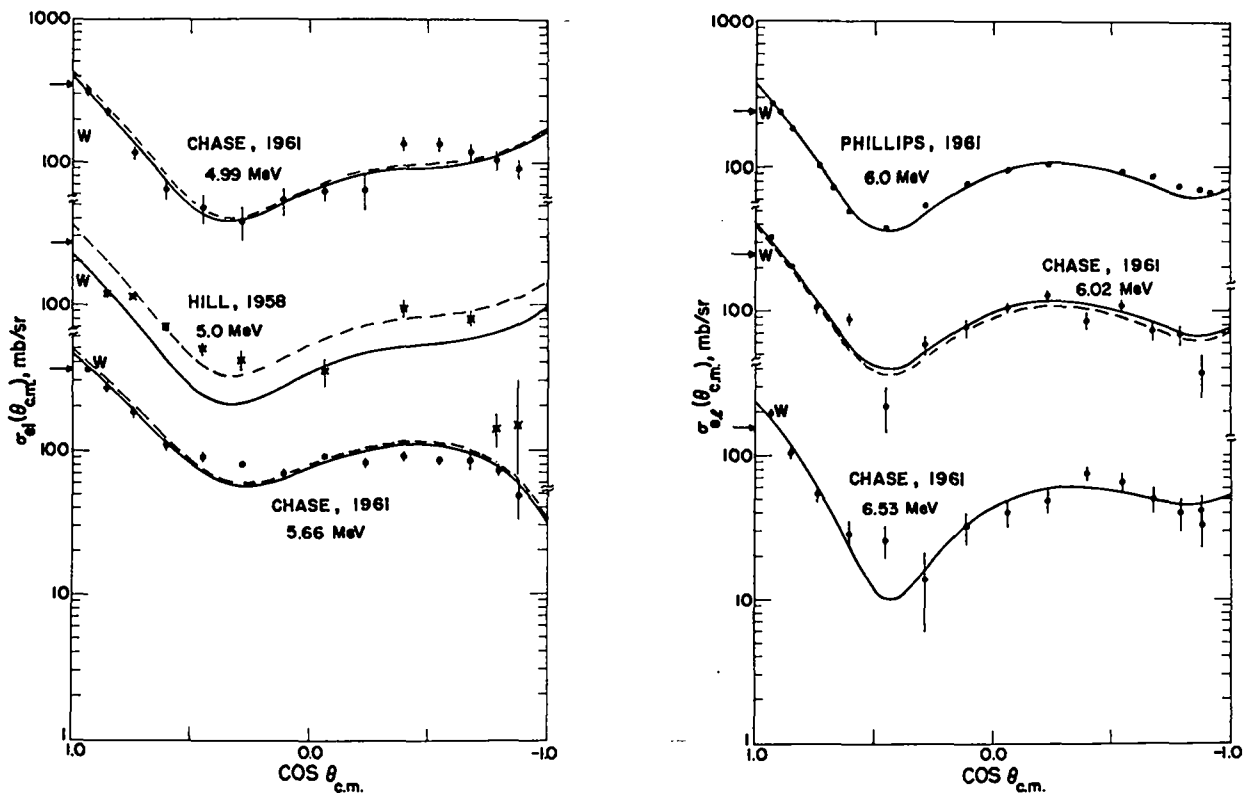


Fig. 38. Measured and evaluated angular distributions for elastic scattering between 4.99 and 6.53 MeV. The solid curves represent the evaluated shapes normalized to the measurements; the dashed curves give the same shapes normalized to the evaluated elastic cross sections. Wick's limit is indicated by the arrows at the left margin.

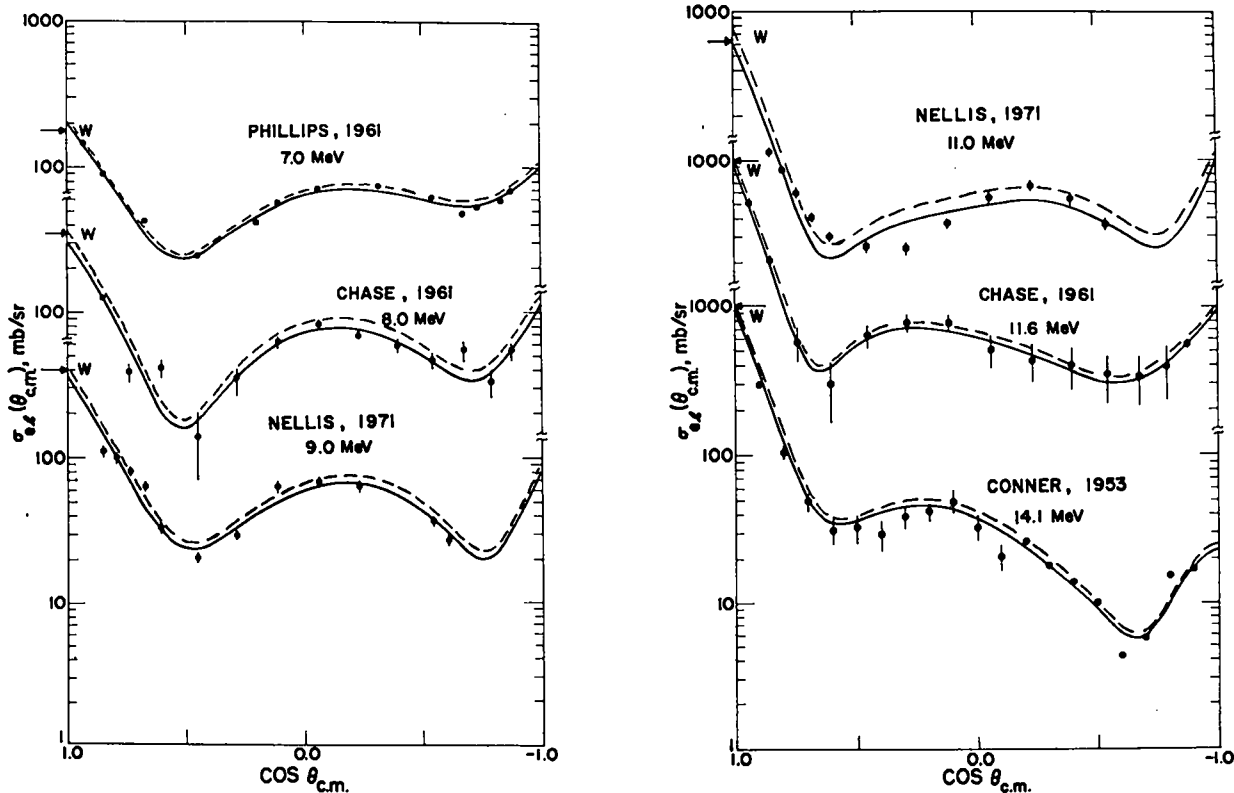


Fig. 39. Measured and evaluated angular distributions for elastic scattering between 7.0 and 14.1 MeV. See caption to Fig. 38 for details.

although slight forward-peaking is seen in the 14-MeV measurements (Ba63, Mc66a).

A complete analysis of the  $(n, n')$  angular distributions should include the results described above, together with all available  $^{16}\text{O}(p, p')$  angular distribution data. We did not make such an analysis for this evaluation, and the inelastic neutron angular distributions are assumed to be isotropic throughout. These results are regarded as preliminary, and improvements are planned for the future.

### 3.3. Secondary-Photon Angular Distributions

The angular distributions of all photons were assumed isotropic in the evaluation. This assumption is known to be invalid for the 6.13-MeV photon at 7.5 MeV, where the measurement of Drake et al. (Dr70) indicates pronounced forward-peaking, with  $\sigma(0^\circ)/\sigma(90^\circ)$  being roughly equal to 2.2. Similarly, near 14 MeV the results of Kozlowski et al. (Ko65) and Buchanan et al. (Bu71) establish  $\sigma(0^\circ)/\sigma(90^\circ)$  to be approximately 1.5. Since the 6.13-MeV photon is very important in the million-electron-volt neutron

energy region and since knowledge of the angular distribution is needed to evaluate the integrated cross section properly, the results given in this evaluation are regarded as tentative, and future work including theoretical considerations is planned.

The results of Morgan et al. (Mo64)\* indicate that the assumption of isotropy is reasonably valid at 14.8 MeV for the 2.74-, 3.09-, 3.68-, 3.85-, 4.44-, 6.92-, and 7.12-MeV photons.

## 4. DISCUSSION

We have mentioned several areas where the present evaluation is deficient and improvements are needed. The most important of these are the 6.13-MeV photon angular distributions, which also affect the  $(n, n')$  and  $(n, n'\gamma)$  cross sections inferred from

\*The data of Morgan et al. (Mo64) are superseded by the results of Buchanan et al. (Bu71); the latter reference, however, contains explicit data only on the angular distribution of the 6.13-MeV photon.

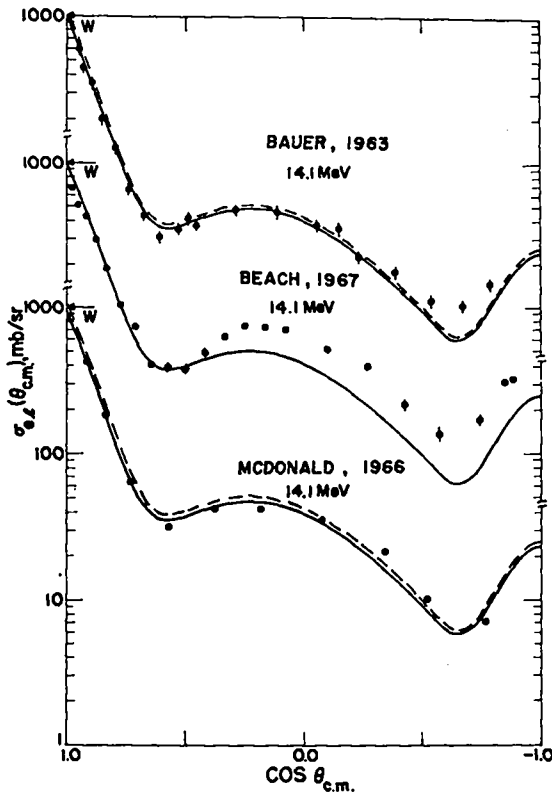


Fig. 40. Measured and evaluated angular distributions for elastic scattering at 14.1 MeV. See caption to Fig. 38 for details.

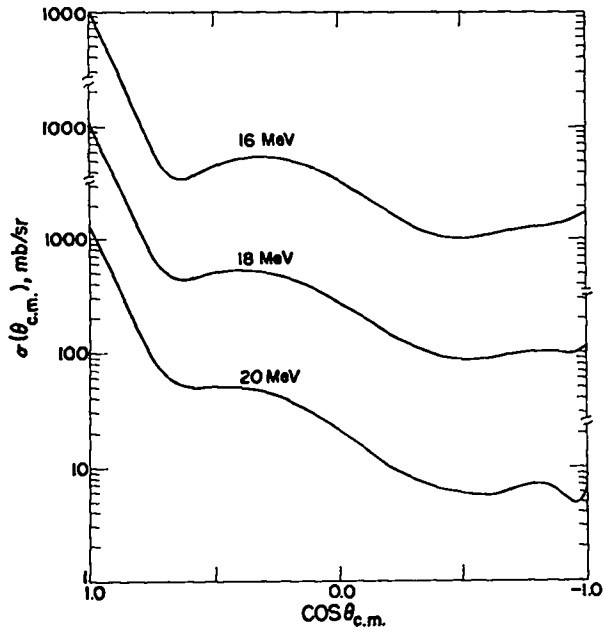


Fig. 41. Evaluated angular distributions for elastic scattering at 16, 18 and 20 MeV.

TABLE V  
ESTIMATED ERRORS IN THE EVALUATED OXYGEN CROSS SECTIONS

Cross Section	ENDF/B Designation	Neutron Energy								
		Thermal	0.1 MeV	1 MeV	3 MeV	5 MeV	8 MeV	11 MeV	14 MeV	20 MeV
Total <sup>a</sup>	MF=3, MT=1	± 4%	± 4%	± 1%	± 1%	± 1%	± 1%	± 1%	± 1%	± 1%
Elastic <sup>a</sup>	MF=3, MT=2	4%	4%	1%	1%	3%	6%	15%	10%	20%
Nonelastic	MF=3, MT=3	14%	order of magnitude	order of magnitude	20%	20%	25%	30%	20%	30%
Total (n,n')	MF=3, MT=4	-	-	-	-	-	30%	30%	30%	30%
Discrete (n,n')	MF=3	-	-	-	-	-	30%	30%	30%	30%
E <sub>x</sub> ( <sup>16</sup> O) < 13 MeV	MT=51 - 70	-	-	-	-	-	30%	30%	30%	30%
Discrete (n,n')	MF=3	-	-	-	-	-	-	-	-	50%
E <sub>x</sub> ( <sup>16</sup> O) > 13 MeV	MT=71 - 89	-	-	-	-	-	-	-	-	50%
(n,γ)	MF=3 MT=102	14%	lower limit only							
(n,p)	MF=3, MT=103	-	-	-	-	-	-	20%	20%	20%
(n,d)	MF=3, MT=104	-	-	-	-	-	-	50%	30%	50%
(n,α)	MF=3, MT=107	-	-	-	20%	20%	20%	20%	20%	20%
Total (n,xy)	MF=13, Sum of MT=4, 22, 102, 103, 107	-	-	-	-	-	30%	30%	30%	30%
Individual (n,xy) lines	MF=13 MT=4, 22, 102, 103, 107	-	-	-	-	-	30%	30%	30%	30%

<sup>a</sup>The error in the total and elastic cross sections near the minimum at 2.35 MeV is ± 1% or ± 0.015 b, whichever is larger.

the photon measurements. Areas involving the inelastic neutron angular distributions and the elastic scattering angular distributions below  $\sim 8$  MeV also need improving. The KAPL evaluation (S165) was used for the latter below 6 MeV, and a detailed resonance-theory analysis incorporating more recent measurements would improve the data set. Finally, more careful reaction-theory calculations should lead to improvements in the inelastic neutron cross sections at higher energies.

A summary of the estimated uncertainties in the various cross sections is given in Table V at several representative neutron energies. The estimates are rough and are not expected to hold true in detail. In addition, the errors are averaged over the structure in the cross sections, and allowance for unknown structure is not included. Time-of-flight spectra of neutrons emerging from liquid oxygen spheres pulsed by 14-MeV neutrons have been calculated by Harris et al. (Ha71) using the present data set and compared

to the experimental measurements of Hansen et al. (Ha70). The calculations, made with the multigroup Monte Carlo code ANDY, agree reasonably well with the measurements, considering the uncertainties associated with the calculation and the cross-section errors given in Table V.

#### ACKNOWLEDGMENTS

We wish to thank C. L. Dunford for performing the COMNUC calculations used in this work and T. A. Pitterle for considerable assistance in evaluating the (n,p) and (n, $\alpha$ ) cross sections. We also wish to thank L. Stewart for many useful comments, and are very grateful to D. M. McClellan, C. I. Baxman, and N. Haines for their help with the clerical tasks needed for this study. Finally, we gratefully acknowledge the contributions of the many authors who provided us with their experimental results in advance of publication.

#### REFERENCES

- Ad49 R. K. Adair, H. H. Barschall, C. K. Bockelman, and O. Sala, "Total Cross Section of Be, O, Na, and Ca for Fast Neutrons," *Phys. Rev.* 75, 1124 (1949).
- Aj59 F. A. Ajzenberg-Selove, and T. Lauritzen, "Energy Levels of Light Nuclei VI," *Nucl. Phys.* 11, 1 (1959).
- Aj70 F. Ajzenberg-Selove, "Energy Levels of Light Nuclei A=13-15," *Nucl. Phys.* A152, 1 (1970).
- Aj71 F. Ajzenberg-Selove, "Energy Levels of Light Nuclei A=16-17," *Nucl. Phys.* A166, 1 (1971).
- Ba63 R. W. Bauer, J. D. Anderson, and L. J. Christensen, "Scattering of 14 MeV Neutrons From Nitrogen and Oxygen," *Nucl. Phys.* 47, 241 (1963).
- Be67 P. L. Beach, R. W. Finlay, R. L. Cassola, and R. D. Koschel, "Elastic Scattering of Neutrons From O and Ar to 14.0 MeV," *Phys. Rev.* 156 1201 (1967).
- Bo63 V. N. Bochkarev and V. V. Nefedov, "A Scintillation  $\gamma$ -Ray Spectrometer with Fast Neutron Discrimination," *Pribory i Tek. Eks.* 6, 1018 (1963).
- Bo63a M. Bormann, S. Cierjacks, E. Fretwurst, K. J. Giesecke, H. Neuert, and H. Pollehn, "Untersuchungen über die Energieabhängigkeit von Kernreaktionen mit Neutronen im Energiebereich zwischen 12 und 19 MeV," *Z. Physik* 174, 1 (1963).
- Bo67 M. Bormann, F. Dreyer, H. Neuert, I. Riehle, and V. Zielinski, "Cross-Sections of Some (n,p), (n,t), and (n, $\alpha$ ) Reactions in the Nitrogen Energy Region 13-19 MeV," *Conference on Nuclear Data, Paris*, (International Atomic Energy Agency, Vienna, 1967) (1966), p. 225.
- Br61 O. D. Brill, N. A. Vlasov, S. P. Kalinen, and L. S. Sokolov, "Cross Section of the (n,2n) Reaction in  $C^{12}$ ,  $N^{14}$ ,  $O^{16}$ , and  $F^{19}$  in the Energy Interval 10-37 MeV," *Sov. Phys.--Dokl.* 6, 24 (1961).
- Bu71 P. S. Buchanan, D. O. Nellis, and W. E. Tucker, "A Compilation of Cross Sections and Angular Distributions of Gamma Rays Produced by Neutron Bombardment of Various Nuclei," *Nuclear-Chicago Corp., Austin, Texas, report ORO-2791-32* (1971).
- Ca60 R. L. Caldwell, W. R. Mills, Jr., and J. B. Hickman, Jr., "Gamma Radiation From Inelastic Scattering of 14-MeV Neutrons by the Common Earth Elements," *Nucl. Sci. Eng.* 8, 173 (1960).
- Ch61 L. F. Chase, Jr., R. V. Smith, R. G. Johnson, F. J. Vaughn, and M. Walt, "Fast Neutron Cross Sections of Oxygen and Nitrogen," *Air Force Weapons Laboratory report AFSWC-TR-61-15* (1961).
- Ci68 S. Cierjacks, P. Forti, D. Kopsch, L. Kropp, J. Nebe, and H. Unseld, "High Resolution Total Cross Sections between 0.5 - 30 MeV," *Kernforschungszentrum report KFK-1000* (1968).

- C171 S. Cierjacks, private communication (1971).
- C169 G. Clayeux and G. Grenier, "Spectres de renvoi des gamma produits par des neutrons de 14.1 MeV," Commissariat a l'Energie Atomique report CEA-R-3807 (1969).
- Co53 J. P. Conner, "A Cloud-Chamber Study of the Scattering of Fast Neutrons in Oxygen," Phys. Rev. 89, 712 (1953).
- Da63 E. A. Davis, T. W. Bonner, D. W. Worley, Jr., and R. Bass, "Disintegration of  $O^{16}$  and  $Cl^{35}$  by Fast Neutrons," Nucl. Phys. 48, 169 (1963).
- Da68 D. Dandy, J. L. Wankling, and C. J. Parnell, "The Cross Section for the  $^{16}O(n,\alpha)^{13}C$  Reaction for Neutron Energies in the Range 7-12 MeV," Atomic Weapons Research Establishment report AWRE O-60/68 (1968).
- De60 J. A. DeJuren and R. W. Stooksberry, "Measurement of the  $O^{16}(n,p)N^{16}$  Cross Section at 14.7 MeV," Phys. Rev. 120, 901 (1960).
- De62 J. A. DeJuren, R. W. Stooksberry, and M. Wallis, "Measurement of the  $O^{16}(n,p)N^{16}$  Cross Section from 11 to 19 MeV," Phys. Rev. 127, 1229 (1962).
- D167 A. S. Divatia, K. K. Sekharan, and M. K. Mehta, " $^{16}O(n,\alpha)^{13}C$  Reaction Cross-Sections from the  $^{13}C(\alpha,n)^{16}O$  Reaction," Conference on Nuclear Data, Paris, (International Atomic Energy Agency, Vienna, 1967), p. 233.
- D170 J. K. Dickens and F. G. Perey, "The  $^{16}O(n,xy)$  Reaction for  $6.7 \leq E_n \leq 11$  MeV," Nucl. Sci. Eng. 40, 283 (1970).
- Dr70 D. M. Drake, J. C. Hopkins, and C. S. Young, "Gamma-Ray-Production Cross Sections for Fast Neutron Interactions with Several Elements," Nucl. Sci. Eng. 40, 294 (1970).
- Du71 C. L. Dunford, private communication (1971); see also C. L. Dunford, "A Unified Model for Analysis of Compound Nucleus Reactions," Atomics International report AI-AEC-12931 (1970).
- En67 F. C. Engesser and W. E. Thompson, "Gamma Rays Resulting from Interactions of 14.7 MeV Neutrons with Various Elements," J. Nucl. Energy 21, 487 (1967).
- Fo58 J. L. Fowler and H. O. Cohn, "Oxygen Differential Neutron Scattering and Phenomenological Nuclear Potentials," Phys. Rev. 109, 89 (1958).
- Fo61 D. B. Fossan, R. L. Walter, W. E. Wilson, and H. H. Barschall, "Neutron Total Cross Sections of Be,  $B^{10}$ , B, C, and O," Phys. Rev. 123, 209 (1961); see also J. C. Davis and F. T. Noda, "Neutron Energy Determinations," Nucl. Phys. A134, 361 (1969).
- Fo64 J. L. Fowler and C. H. Johnson, "The Scattering of 3 to 4 MeV Neutrons from  $O^{16}$ ," Oak Ridge National Laboratory report ORNL-3582 (1964), p. 90.
- Fo70 J. L. Fowler and C. H. Johnson, "Differential Scattering of Neutrons at Narrow Levels in  $^{17}O$ ," Phys. Rev. C2, 124 (1970).
- Fo71 D. G. Foster, Jr., and D. W. Glasgow, "Neutron Total Cross Sections, 2.5-15 MeV. I. Experimental," Phys. Rev. C3, 576 (1971).
- Fo71a J. L. Fowler, C. H. Johnson, F. X. Haas, and R. M. Freezel, "The Neutron Total Cross Section of  $^{16}O$  and  $^{40}Ca$ ," Oak Ridge National Laboratory report CCNF-710301 (1971), p. 179.
- Ha59 H. E. Hall and T. W. Bonner, "Gamma Radiations from Inelastic Scattering of Fast Neutrons in  $Cl^{35}$ ,  $N^{14}$ , and  $O^{16}$ ," Nucl. Phys. 14, 295 (1959).
- Ha70 L. F. Hansen, J. D. Anderson, E. Goldberg, J. Kammerdiener, E. Plechaty, and C. Wong, "Predictions for Neutron Transport in Air, Based on Integral Measurements in Nitrogen and Oxygen at 14 MeV," Nucl. Sci. Eng. 40, 262 (1970); L. F. Hansen, J. D. Anderson, J. L. Kammerdiener, and C. Wong, "Sensitivity of Monte Carlo Calculations to the Neutron Cross Sections for Neutron Transport in Nitrogen and in Air," Lawrence Livermore Laboratory report UCRL-51031 (1971).
- Ha71 D. R. Harris, D. R. Koenig, and W. Preeg, "Multigroup Monte Carlo and  $S_N$  Methods for Air Transport," Seminar on Radiation Transport in Air, November, 1971, Radiation Shielding Information Center, Oak Ridge, Tenn. (ORNL-RSIC-33) p. 209.
- Hi58 R. W. Hill, "Angular Distributions of Elastic Scattering of 5-MeV Neutrons," Phys. Rev. 109, 2105 (1958).
- Hs67 Y.-C. Hsu, C.-Y. Huang, and C.-C. Chang, "Angular Distributions of Alpha Particles from the Reaction  $^{16}O(\alpha,\alpha)^{13}C$  at  $E_n=14.1$  MeV," Nucl. Phys. A104, 677 (1967).
- Hu62 W. Hunzinger and P. Huber, "Differentieller Wirkungsquerschnitt von Sauerstoff-16 für Neutronen im MeV-Energiebereich," Helv. Phys. Acta 35, 351 (1962).
- Jo48 W. B. Jones, Jr., "Slow Neutron Cross Section of H," Phys. Rev. 74, 364 (1948).
- Jo67 C. H. Johnson and J. L. Fowler, "Scattering of Neutrons from  $^{16}O$  in the 2.2- to 4.2-MeV Energy Range," Phys. Rev. 162, 890 (1967).
- Ju63 E. T. Journey and H. T. Motz, "Thermal Neutron Capture in D and  $O^{16}$ ," Argonne National Laboratory report ANL-6797 (1963), p. 236.
- Ju71 E. T. Journey, private communication (1971).
- Ka62 J. Kantele and D. G. Gardner, "Some Activation Cross Sections for 14.7 MeV Neutrons," Nucl. Phys. 35, 353 (1962).

- Ka71 J. Kalyna, I. J. Taylor, and L. J. Lidofsky, "Total Neutron Cross Section of  $^{16}\text{O}$  at 2.37 MeV," submitted to Third Conference on Neutron Cross Sections and Technology, Knoxville (1971), Abstract No. II.26; and private communications (1971).
- Ko65 T. Kozlowski, W. Kusch, and J. Wojtkowska, "Gamma Rays from Inelastic Scattering of 14.1 MeV Neutrons on  $\text{C}^{12}$  and  $\text{O}^{16}$ ," Polish Academy of Sciences report INR-661/IA/PL (1965).
- La60 R. O. Lane, A. S. Langsdorf, Jr., J. E. Monahan, and A. J. Elwyn, "Tables of Differential Cross Sections for Scattering of Neutrons from Various Nuclei," Argonne National Laboratory report ANL-6172 (1960); see also Ann. Phys. (N.Y.) 12, 135 (1961).
- Li52 A. B. Lillie, "The Disintegration of Oxygen and Nitrogen by 14.1-MeV Neutrons," Phys. Rev. 87, 716 (1952).
- Li66 D. Lister and A. Sayres, "Elastic Scattering of Neutrons from Carbon and Oxygen in the Energy Range 3.0 to 4.7 MeV," Phys. Rev. 143, 745 (1966).
- Lo62 G. N. Lovchikova, "Scattering of Fast Neutrons on Nuclei," Soviet J. At. Energy 13, 648 (1962).
- Ma54 H. C. Martin, "Cross Sections for the  $\text{O}^{16}(\text{n,p})\text{N}^{16}$  Reaction from 12 to 18 MeV," Phys. Rev. 93, 498 (1954).
- Ma62 J. P. Martin and M. S. Zucker, "Differential Cross Section and Polarization Angular Distributions for  $\text{O}^{16}(\text{n,n}')\text{O}^{16}$ ," Bull. Am. Phys. Soc. 7, 72 (1962), Abstract V5.
- Ma65 J. H. E. Mattauch, W. Thiele, and A. H. Wapstra, "1964 Atomic Mass Table," Nucl. Phys. 67, 1 (1965).
- Mc66 W. N. McDicken and W. Jack, "The Reactions  $^{20}\text{Ne}(\text{n},\alpha)^{17}\text{O}$  and  $^{16}\text{O}(\text{n},\alpha)^{13}\text{C}$  Using 14 MeV Neutrons," Nucl. Phys. 88, 457 (1966).
- Mc66a W. J. McDonald, J. M. Robson, and R. Malcolm, "Scattered Neutrons and Gamma Rays from the  $^{16}\text{O}(\text{n},\text{n}')^{16}\text{O}$  Reaction at  $E_n=14.1$  MeV," Nucl. Phys. 75, 353 (1966).
- Me49 E. Melkonian, "Slow Neutron Velocity Spectrometer Studies of  $\text{O}_2$ ,  $\text{N}_2$ ,  $\text{A}$ ,  $\text{H}_2$ ,  $\text{H}_2\text{O}$ , and Seven Hydrocarbons," Phys. Rev. 76, 1750 (1949).
- Mi66 B. Mitra and A. M. Ghose, " $(\text{n,p})$  Cross Sections of Some Low Z Nuclei for 14.8 MeV Neutrons," Nucl. Phys. 83, 157 (1966).
- Mo64 I. L. Morgan, J. B. Ashe, and D. O. Nellis, "Angular Distribution of Gamma Rays from C, O, and N at  $E_n=14.8$  MeV," in Nuclear Physics Division Annual Progress Report (Texas Nuclear Corp., Austin, 1964), p. 156.
- Ne71 D. O. Nellis, P. S. Buchanan, T. C. Martin, W. E. Tucker, G. H. Williams, and A. J. Wolf-ram, "Neutron Scattering and Gamma-Ray Production Cross Sections for N, O, Al, Si, Ca, and Fe," private communication (1971).
- Ny70 K. Nyberg, B. Jönsson, and I. Bergqvist, "High Resolution Measurements of Gamma Rays Produced by 15 MeV Neutrons," Aktiebolaget Atomenergi report AE-INSN-2 (1970), Sect. V.
- Ok55 A. Okazaki, "Scattering of Polarized Neutrons by Heavy Nuclei," Phys. Rev. 99, 55 (1955).
- Or70 V. J. Orphan, C. G. Hoot, and J. Joh, "Gamma-Ray Production Cross Sections for the  $^{16}\text{O}(\text{n},\text{xy})$  Reaction from 6.35- to 16.52-MeV Neutron Energy," Nucl. Sci. Eng. 42, 352 (1970).
- Pa53 E. B. Paul and R. L. Clarke, "Cross-Section Measurements of Reactions Induced by Neutrons of 14.5 MeV Energy," Can. J. Phys. 31, 267 (1953).
- Ph61 D. D. Phillips, private communication to R. J. Howerton (1961).
- Pr66 R. Prasad, D. C. Sarkar, and C. S. Khurana, "Measurement of  $(\text{n,p})$  and  $(\text{n},\alpha)$  Reaction Cross Sections at 14.8 MeV," Nucl. Phys. 85, 476 (1966).
- Sc71 R. B. Schwartz, private communication (1971).
- Se55 J. Seitz and P. Huber, "Wirkungsquerschnitt der  $\text{O}^{16}(\text{n},\alpha)\text{C}^{13}$ -Reaktion für schnelle Neutronen," Helv. Phys. Acta 28, 227 (1955).
- Se62 K. W. Seemann and W. E. Moore, "The  $\text{O}^{16}(\text{n,p})\text{N}^{16}$  Cross Section from 12.6 to 16.3 MeV," Knolls Atomic Power Laboratory report KAPL-2214 (1962).
- Si68 I. Sick, E. Baumgartner, P. Huber, and Th. Stambach, "Messung des differentiellen Wirkungsquerschnitts der Reaktion  $^{16}\text{O}(\text{n},\alpha)^{13}\text{C}$  im Energiegebiet von 14.8 - 18.8 MeV," Helv. Phys. Acta 41, 573 (1968).
- Sl65 E. L. Slaggie and J. T. Reynolds, " $\text{O}^{16}$  Fast Neutron Cross Sections and Legendre Moments below 15.0 MeV," Knolls Atomic Power Laboratory report KAPL-M-6452 (1965).
- Wa57 R. B. Walton, J. D. Clement, and F. Boreli, "Interaction of Neutrons with Oxygen and a Study of the  $\text{C}^{13}(\alpha,\text{n})\text{O}^{16}$  Reaction," Phys. Rev. 107, 1065 (1957).
- Wi43 G. C. Wick, Atti reale accad. Italia, Mem. classes sci. fis., mat. e nat. 13, 1203 (1943); see also J. H. Coon, R. W. Davis, H. E. Felt-hauser, and D. B. Nicodemus, "Scattering of 14.5-MeV Neutrons by Complex Nuclei," Phys. Rev. 111, 250 (1958), and L. Stewart, "Evaluated Neutron Cross Sections for Tritium," Los Alamos Scientific Laboratory report LA-3270 (1965).

Yo72 P. G. Young and D. G. Foster, Jr., "An Evaluation of the Neutron and Gamma-Ray Production Cross Sections for Nitrogen," Los Alamos Scientific Laboratory report LA-4725 (1972).

Yo72a P. G. Young and D. G. Foster, Jr., "A Preliminary Evaluation of the Neutron and Photon Production Cross Sections for Aluminum," Los Alamos Scientific Laboratory report LA-4726 (1972).